nature water

Analysis

https://doi.org/10.1038/s44221-025-00522-8

Hydroclimate and landscape diversity drive highly variable greenhouse gas emissions from tropical and subtropical inland waters

Received: 17 October 2024

Accepted: 10 September 2025

Published online: 17 October 2025

Check for updates

Clément Duvert[1,2] ✉, Alberto V. Borges[3] ✉, Elisa Calamita[4,5], Gerard Rocher-Ros[6,7], Annika Linkhorst[8], Judith A. Rosentreter[9], Shaoda Liu[10], Pierre Taillardat[11], Katrin Attermeyer[12,13], Tonya DelSontro[14], Loris Deirmendjian[15], Alicia A. Dixon[16], Charlotte Grasset[17], Allison M. Herreid[18], Luke C. Jeffrey[9], Lediane Marcon[19,20], Ricky M. Mwanake[21], José R. Paranaíba[22], Lishan Ran[23], Adam T. Rexroade[1], Vanessa Solano[1,24], Francesco Ulloa-Cedamanos[1], Jilong Wang[25], Keridwen M. Whitmore[26], Liwei Zhang[27], Carla López-Lloreda[28], Marcia N. Macedo[29,30], Diana Oviedo-Vargas[31], Diego A. Riveros-Iregui[26] & Nicholas S. Marzolf[32] ✉

(Sub)tropical inland waters are important greenhouse gas (GHG) sources, yet limited observations have long hindered broad analyses of GHG variability across this diverse region. Here, through a meta-analysis, we have examined the rates and drivers of GHG emissions from flowing and standing (sub)tropical inland waters. We find considerable spatial variation in fluxes, largely related to differences in hydroclimate, geomorphology, land cover and human disturbance. Flowing waters emit more carbon dioxide ($3{,}387^{5{,}702}_{2{,}121}$ $TgCO_2\ yr^{-1}$, expressing $median^{third\ quartile}_{first\ quartile}$), methane ($10.6^{28.8}_{0.1}$ $TgCH_4\ yr^{-1}$) and nitrous oxide ($0.62^{1.10}_{0.35}$ $TgN_2O\ yr^{-1}$) than standing waters (114^{219}_{73} $TgCO_2\ yr^{-1}$, $5.4^{9.1}_{2.1}$ $TgCH_4\ yr^{-1}$ and $0.03^{0.05}_{0.02}$ $TgN_2O\ yr^{-1}$, respectively). (Sub)tropical inland waters release $4{,}238^{7375}_{2473}$ $TgCO_2$-equivalents annually, with first- to third-order streams contributing 75% of riverine emissions and lakes larger than 100 km^2 contributing 59% of standing water emissions. Our results suggest emissions from (sub)tropical waters are 29–72% lower than earlier estimates, a downward revision with important implications for global GHG budgets.

Inland waters, including streams, rivers, lakes, ponds and reservoirs, are active biogeochemical reactors that receive, store, transport and process terrestrial carbon (C) and nitrogen (N). These reactions generate substantial amounts of greenhouse gases (GHGs), such as carbon dioxide (CO_2), methane (CH_4) and nitrous oxide (N_2O), which are subsequently emitted into the atmosphere[1–8]. Estimates of GHG emissions from global inland waters have been revised upwards in recent years, and evidence indicates that these emissions have changed considerably over the past centuries due to human activities[4,5,9]. However, estimating the current flux at both regional and global scales remains highly uncertain, with challenges arising from strong variability in time and space across multiple scales, limited observations in certain regions of the world and large uncertainties regarding the spatial extent of inland waters[6,10].

Despite these remaining uncertainties, the importance of tropical inland waters in global GHG emissions has become increasingly

A full list of affiliations appears at the end of the paper. ✉e-mail: clem.duvert@cdu.edu.au; alberto.borges@uliege.be; nick.marzolf@jonesctr.org

apparent[2,7,11–14]. Recent modelling suggests that approximately 56% and 52% of riverine CO_2 and CH_4 emissions, respectively, originate from the tropics, which make up only about 43% of the global river surface area[7,14]. Tropical and subtropical lakes contribute roughly half of global lake CH_4 emissions, despite representing only 13% of total lake surface area[15]. While N_2O fluxes remain poorly constrained globally[10], major river networks in the (sub)tropics, such as the Amazon, Ganges, Niger and Yangtze, have been identified as potential key contributors to global riverine N_2O emissions[4,16], although some large near-pristine rivers, such as those within the Congo River network, seem to be modest N_2O sources[13]. The N_2O emissions from tropical lakes, in contrast, can be marginal[17,18].

One limitation to the prevailing assumption that the tropics are hotspots for inland water GHG emissions is that it may omit the nuances and complexity of this vast region. The tropics encompass a myriad of subclimates, landforms, vegetation types and varying degrees of human disturbance, but this diversity has not been reflected in global datasets, which until recently were based primarily on observations from the Amazon basin[2,19,20]. Due to limited spatial coverage and a lack of consistent seasonal sampling, the tropics have often been treated as a constant and homogeneous hotspot of GHG emissions, with global studies overlooking the potentially wide range of GHG concentrations and fluxes across diverse (sub)tropical inland waters[2,19,20]. Over the past 10 years, research on tropical GHG emissions has expanded substantially (Extended Data Fig. 1), leading to a much more detailed representation of tropical ecosystems and their contribution to global inland water emissions. New studies have highlighted tropical heterogeneity at regional or continental scales[12,18,21], yet a global synthesis integrating emissions from all three GHGs and both flowing and standing inland waters is still lacking.

In this study, we aimed to develop a nuanced understanding of the patterns and drivers of tropical inland water GHG emission variability. We leveraged the growing number of measurements across the tropics, which now offer better spatial coverage and more representative seasonal sampling, together with recent improvements in geospatial datasets of inland water surface areas[22–25], to provide an updated estimate of these emissions. We also examined geographical disparities and drivers of GHG emissions, and identified regions and ecosystems that still have substantial observation gaps. Given the ongoing climate change in temperate and subtropical ecosystems[26], we adopted a broad spatial coverage that includes subtropical inland waters to anticipate future scenarios of GHG emissions. As such, we refer to the tropics and subtropics collectively as the '(sub)tropics', with cut-off latitudes of 34° S and 34° N.

Geographic coverage and patterns of GHG data

We partitioned the (sub)tropics into five climate zones based on a simplified version of the updated Köppen–Geiger classification[27]: (1) humid tropics (sometimes called rainforest tropics or wet tropics), (2) wet-dry tropics (also referred to as savanna tropics or seasonally dry tropics), (3) arid and semi-arid (sub)tropics, (4) humid subtropics and (5) highland (or mountain) (sub)tropics (Extended Data Fig. 2). We explored the differences in GHG concentrations and fluxes across these five climate zones for both flowing (that is, streams and rivers) and standing (that is, lakes, reservoirs and ponds) waterbodies. We based our meta-analysis on over 500 peer-reviewed articles, with the majority (65%) of the data collected in the past 10 years (see Methods and Extended Data Fig. 1). Spatial coverage was uneven across the (sub) tropics (Fig. 1a,b, Extended Data Fig. 3 and Supplementary Figs. 4–7), with the highest density of measurements in the highland tropics, southeastern China (which covers much of the humid subtropics) and, to a lesser extent, the Amazon and Congo basins (which cover much of the humid tropics). In contrast, (semi)arid regions had notably less observations. The distribution of surface areas across size classes and climate zones (Fig. 1c,d) revealed that standing waterbodies larger than 100 km^2 accounted for the majority (70%) of the total surface area, with a particularly large share located in the wet-dry tropics (26%). For flowing waters, first- to third-order streams contributed the most to the total surface area (51%), with the majority (32%) located in the humid and wet-dry tropics combined.

The concentrations and fluxes of CO_2 were both consistently higher than those of CH_4 (considered in its diffusive form unless otherwise specified) and N_2O across both flowing and standing waterbodies (Fig. 1e,f). For rivers, CO_2 and CH_4 emissions showed similar patterns across climate zones, with the highest area-weighted fluxes observed in the humid, wet-dry and highland tropics, while N_2O emissions peaked in the highland tropics. Low-order streams had significantly higher GHG fluxes than high-order rivers, consistent with recent global studies on all three GHGs[4,7,9,14,16]. In standing waterbodies, the CO_2 and CH_4 concentrations tended to decrease with increasing surface area, but differences were rarely significant. While previous work reported decreasing CO_2 and CH_4 fluxes with larger surface area[2,28–30], our dataset did not show consistent size-related patterns in fluxes due to high within-group variability. Cross-climate differences in standing waters were generally weak, except for N_2O, which was higher in the humid subtropics and lower in the wet-dry tropics than in other climate zones.

Humid and wet-dry tropics dominate riverine emissions

Our upscaling approach suggests that (sub)tropical streams and rivers emitted $3{,}387^{5{,}702}_{2{,}121}$ $TgCO_2\ yr^{-1}$ (representing median $^{\text{third quartile}}_{\text{first quartile}}$), $10.6^{28.8}_{0.1}$ $TgCH_4\ yr^{-1}$ and $0.62^{1.10}_{0.35}$ $TgN_2O\ yr^{-1}$ (Table 1). Despite representing ~62% of the wetted river surface area of the (sub)tropics, the combined humid and wet-dry tropical zones accounted for 77%, 81% and 67% of the (sub)tropical riverine CO_2, CH_4 and N_2O fluxes, respectively. In contrast, the arid and semi-arid (sub)tropics contributed 11%, 9% and 14% to the riverine CO_2, CH_4 and N_2O fluxes, despite hosting a larger proportion (~20%) of the total wetted river surface area. The remaining

Fig. 1 | Spatial distribution and characteristics of GHG concentration and flux measurements across (sub)tropical climate zones. a,**b**, Locations of measurements in flowing (**a**) and standing (**b**) waterbodies. Each marker corresponds to a site with any GHG concentration and/or flux measurement. **c**,**d**, Estimated wetted surface areas of (sub)tropical flowing (**c**) and standing (**d**) waters across climate zones. **e**,**f**, Distributions of CO_2, diffusive CH_4 and N_2O concentrations and fluxes from flowing (**e**) and standing (**f**) waters, shown as a function of stream order and lake/reservoir surface area, respectively. The *y*-axis labels in **e** and **f** reflect log-transformed values (for example, $-3 = 10^{-3}$). Fluxes that were estimated as the product of concentration measurements, and gas transfer velocity estimates (see Methods) are included in the plots. Coloured markers represent the median value for each stream order or lake size class. Letters indicate significant differences between the medians of each climate zone based on two-sided Kruskal–Wallis and pairwise Wilcoxon rank-sum post hoc tests ($p < 0.01$). Asterisks indicate significant differences across stream orders or size classes within a climate zone based on two-sided Kruskal–Wallis tests (*$p < 0.05$ and **$p < 0.01$; see Methods and Supplementary Tables 11–16). For flowing waters, a constant of 0.1 was added to the N_2O fluxes to visualize the 6.2% (number of observations n_obs = 41) negative values on a log scale. No constant was added to the CO_2 and CH_4 fluxes; 2.2% (n_obs = 60) and 0.6% (n_obs = 12) of the CO_2 and CH_4 flux values are negative and not shown in the plots. For standing waters, constants were added to the CO_2 (+100) and N_2O (+0.01) fluxes to visualize the 21% (n_obs = 56; CO_2) and 36% (n_obs = 35; N_2O) negative values on a log scale. No constant was added to the CH_4 fluxes; 0.9% (n_obs = 3) of the CH_4 flux values are negative and not shown in the plots. Dashed horizontal lines indicate the actual zero threshold. Some stream orders and size classes were merged for visual clarity. Humid, humid tropics; Wet-dry, wet-dry tropics; Arid, (semi) arid tropics and subtropics; Humid sub., humid subtropics; Highland, highland tropics and subtropics (see Extended Data Fig. 2 for the geographic coverage of each climate zone). Here we consider the latitudes between 34° S and 34° N.

https://doi.org/10.1038/s44221-025-00522-8

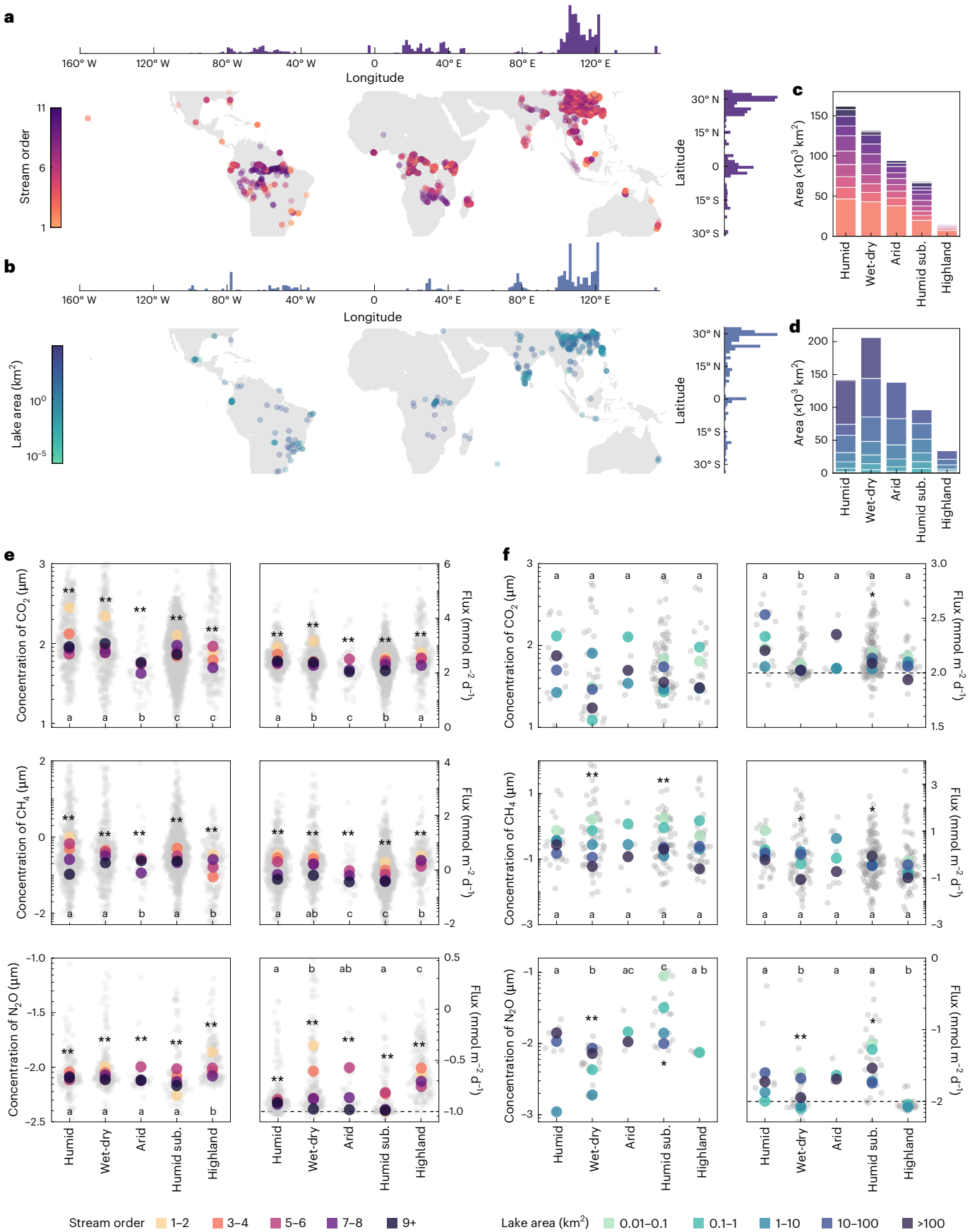

https://doi.org/10.1038/s44221-025-00522-8

Table 1 | Total median riverine GHG emissions for each climate zone of the (sub)tropics

Climate zone	CO_2 flux ($TgCO_2\,yr^{-1}$)	CH_4 diffusive flux ($TgCH_4\,yr^{-1}$)	CH_4 ebullitive flux ($TgCH_4\,yr^{-1}$)	N_2O flux ($TgN_2O\,yr^{-1}$)
Humid tropics	1,353 (854–2,325)	2.20 (1.31–3.40)	2.51 (0.08–6.58)	0.100 (0.054–0.198)
Wet-dry tropics	1,257 (763–2,272)	1.88 (0.95–3.55)	2.03 (−0.06–6.06)	0.316 (0.187–0.589)
(Semi)arid (sub)tropics	363 (239–497)	0.43 (0.27–0.61)	0.50 (0.04–1.22)	0.085 (0.044–0.134)
Humid subtropics	309 (197–440)	0.26 (0.17–0.38)	0.32 (0.03–0.80)	0.084 (0.046–0.132)
Highland (sub)tropics	105 (68–168)	0.21 (0.10–0.33)	0.24 (−0.02–0.63)	0.031 (0.016–0.049)
Total	**3,387 (2,121–5,702)**	**4.98 (2.80–8.27)**	**5.59 (0.06–15.28)**	**0.615 (0.346–1.102)**

Values are based on a bootstrapping approach (see Methods) and the lower and upper bounds in parentheses correspond to the first (Q1) and third (Q3) quartiles, respectively. The CH_4 ebullitive fluxes were estimated from the CH_4 diffusive flux for each site in the database based on the relationship outlined in Rocher-Ros et al.[7]. Further details on the distribution of surface areas per stream order and climate zone are available in Supplementary Table 8.

contributions were from the humid subtropics (9%, 6% and 14% of the riverine CO_2, CH_4 and N_2O fluxes) and the highland (sub)tropics (3%, 4% and 5% of the riverine CO_2, CH_4 and N_2O fluxes).

To assess the contributions of each GHG to the total modelled emission flux in terms of their radiative forcing, we derived CO_2-equivalent fluxes based on the global warming potential of CH_4 and N_2O over 100 years (Fig. 2). The CO_2 flux was the largest component, contributing 91% of the total riverine CO_2-equivalent emissions, while the total (diffusive + ebullitive) CH_4 and N_2O fluxes represented 4% and 5% of this total, respectively. The CO_2 and total CH_4 emissions showed similar differences across climate zones, with dominant contributions from the humid and wet-dry tropics, whereas N_2O emissions were highest in the wet-dry tropics, and almost as high in (semi)arid areas and humid subtropics as in the humid tropics.

Our scaled GHG emission estimates from flowing waters differ substantially from previous estimates. Considering the same cut-off latitudes as ours, our median CO_2 emission flux estimate (3,387 $TgCO_2\,yr^{-1}$) is 29% lower than that from Liu et al.[14] (4,792 $TgCO_2\,yr^{-1}$), whereas the median estimate of Tian et al.[9] (~1,100 $TgCO_2\,yr^{-1}$) is much lower than ours. For the same latitude range, our median total CH_4 emission estimate (10.6 $TgCH_4\,yr^{-1}$) is 45% lower than that of Rocher-Ros et al.[7] (19.1 $TgCH_4\,yr^{-1}$). Our median N_2O estimate (0.62 $TgN_2O\,yr^{-1}$) represents 67–78% of modelled estimates for the entire world[4,8] (0.92 and 0.80 $TgN_2O\,yr^{-1}$, respectively) but is higher than the estimate from another global study[16] (0.23 $TgN_2O\,yr^{-1}$). The discrepancies with previous CO_2 and CH_4 estimates are unlikely to result from differences in river surface area, but instead might reflect our lower gas transfer velocity estimates as we used finer channel slope estimates[24] than previous studies[7,14] (Supplementary Discussion 4). Discrepancies are also likely to reflect differences in upscaling approaches—meta-analysis versus network modelling—and the larger number of empirical measurements included in our synthesis. Compared with earlier work[7,14], we drew on 2.6 times more CO_2 sites and 1.5 times more CH_4 sites, with a stronger emphasis on direct observations rather than modelled values. We are therefore confident that our values are better constrained than previous estimates (Supplementary Discussion 3).

Drivers of riverine emissions differ among GHGs

The humid tropics were the largest emitters of CO_2 and CH_4 ($p < 0.01$; Fig. 2), driven by their extensive wetted surface area (the largest among all climate zones; Supplementary Table 8) and high dissolved GHG concentrations that led to high area-weighted emissions despite relatively low gas transfer velocities (Fig. 1 and Supplementary Tables 9, 10 and 12). The wet-dry tropics ranked second ($p < 0.01$; Fig. 2), with wetted areas and GHG inputs nearly as high as those in the humid tropics and higher gas transfer velocities (Supplementary Table 12b). Wet-dry tropical streams had the highest N_2O emissions ($p < 0.01$; Fig. 2), largely due to high concentrations in low-order streams (Supplementary Table 10). Despite occupying only 3% of the (sub)tropical wetted river surface area (Fig. 1 and Supplementary Table 8) and having low GHG concentrations (Supplementary Table 12b), highland tropical rivers had among the highest area-weighted GHG fluxes ($p < 0.01$; Fig. 1e and Supplementary Table 12a), a result of their higher gas transfer velocities (Supplementary Table 12b), in line with previous studies[31,32]. Conversely, the (semi)arid tropics contributed less, likely due to lower GHG concentrations (Supplementary Table 12a) reflecting limited terrestrial–aquatic connectivity and lower wetland extent[33]. Across all climate zones, low-order streams were key emitters, combining large wetted areas with high GHG inputs (Fig. 1 and Supplementary Tables 8, 9 and 11b). When considered alone, first- to third-order streams accounted for 75% of the total riverine GHG emissions from the entire (sub)tropics, consistent with earlier findings, highlighting the disproportionate role of low-order streams in emissions[4,9,14,16].

To understand the drivers of riverine GHG fluxes at finer spatial scales, we examined the interplay between climate, hydrological and landscape variables. Given the relatively limited number of direct flux measurements, especially for N_2O, we used concentration data instead (see Methods). The positive relationship between flux and concentration across sites (Extended Data Fig. 4) suggests that gas content is a strong control for emissions, which allowed us to assume that the drivers identified for concentrations are similarly relevant for fluxes.

Using a range of catchment predictors, we were able to explain 35–46% of the variance (R^2) in measured GHG concentrations (Fig. 3). While the importance of specific predictors varied across the three GHGs, a common finding was the role of hydrological variables (light-red bars in Fig. 3). Hydrology was at least as important as landscape (pink bars) and climate (purple bars) variables in explaining GHG variations. Discharge, which in this analysis reflects spatial variation across sites (and thus scales positively with stream order) rather than temporal variations within sites, accounted for much of the variability in all GHGs, with higher discharge (that is, larger rivers) leading to lower concentrations. This inverse relationship with discharge is well established for CO_2 (refs. 9,34–36) and has occasionally been reported for CH_4 and N_2O (refs. 37,38). Groundwater depth had a strong negative effect on CO_2 and CH_4 concentrations, confirming the key role of hydrological connectivity and lateral inputs (that is, low groundwater depths) in supplying terrestrial C to tropical streams and rivers[39–42].

Rainfall seasonality negatively correlated with CO_2, supporting our observation that productive regions with a more stable rainfall regime throughout the year (such as the humid tropics) had higher CO_2 inputs. This relationship was also strong for N_2O, but weaker and slightly positive for CH_4. Human footprint[43] was the strongest predictor of N_2O and a relatively important driver of CH_4, with high human disturbance related to high GHG concentrations. Previous studies have linked increases in riverine GHG emissions to human alteration[7,30,44,45], an effect that is greater in lower- to middle-income countries[46], which are prevalent across the (sub)tropics, especially in the wet-dry tropics and humid subtropics.

Peatland extent was a strong predictor of CH_4 and, to a lesser extent, of CO_2, with greater peatland cover associated with higher GHG concentrations. In large, lowland tropical rivers, CO_2 and CH_4 concentrations are often closely linked to wetland extent across the drainage area[11–13,47]. Temperature also influenced riverine CH_4

https://doi.org/10.1038/s44221-025-00522-8

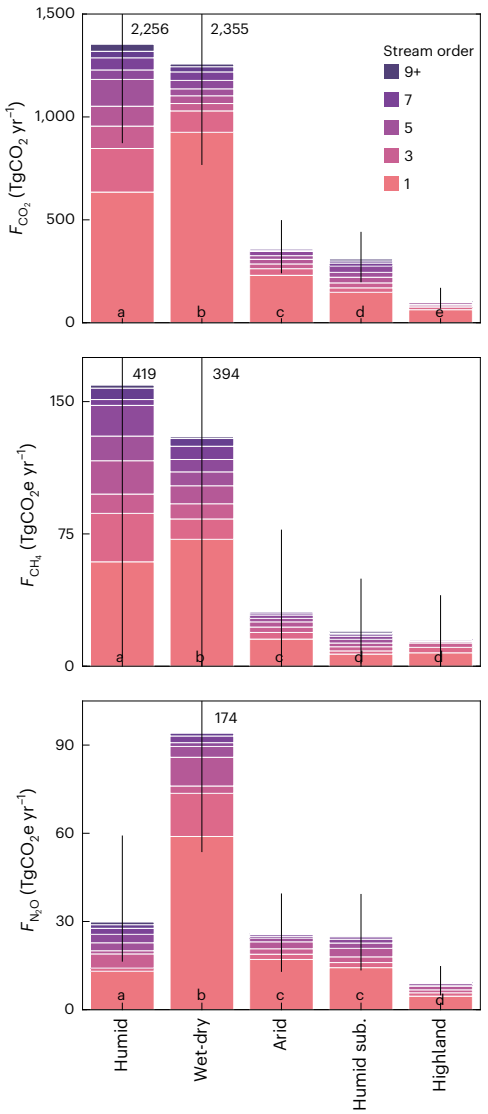

Fig. 2 | Contributions of CO_2, CH_4 and N_2O to the total modelled riverine emission flux. Median fluxes were estimated for each stream order and across different climate zones. Fluxes are expressed as CO_2-equivalents using 100-year global warming potential factors of 34 for CH_4 and 298 for N_2O (ref. 113). CH_4 fluxes include both diffusive and ebullitive fluxes. Error bars indicate the first (Q1) and third (Q3) quartiles based on propagated uncertainties. For clarity, some error bars have been truncated and the corresponding Q3 values are shown. Letters indicate significant differences between climate zones based on two-sided Kruskal–Wallis tests followed by pairwise, two-sided Wilcoxon rank-sum post hoc comparisons with Benjamini–Hochberg correction ($p < 0.01$), applied to bootstrapped flux distributions.

concentrations, consistent with the strong temperature dependency of methanogenesis[48,49]. In contrast, temperature showed a weak negative relation with CO_2. This likely reflects complex interactions between biological and physical drivers, and is not inconsistent with the observation that net heterotrophy in tropical streams is largely independent of temperature variability[21]. In sum, we found that river size and groundwater depth were strongly associated with concentrations (and presumably fluxes) across all GHGs, while peatland extent, human footprint, rainfall seasonality and temperature had gas-specific effects.

Lakes dominate CH_4 emissions, reservoirs a larger source of CO_2 and N_2O

Our upscaling approach suggests that, together, the standing waterbodies of the (sub)tropics released 114^{219}_{73} TgCO$_2$ yr^{-1}, $5.4^{9.1}_{2.1}$ TgCH$_4$ yr^{-1} and $0.03^{0.05}_{0.02}$ TgN$_2$O yr^{-1} (Table 2). Scaled total CH_4 fluxes were twice as high in lakes as in reservoirs, whereas scaled CO_2 and N_2O fluxes were 1.7 and 10 times higher in reservoirs, respectively. Lakes and reservoirs larger than 100 km^2 (that is, our two largest size classes) represented 52%, 40% and 70% of the CO_2, total CH_4 and N_2O emissions, respectively. In contrast, lakes and reservoirs smaller than 1 km^2 (that is, our two smallest size classes) represented only 14%, 29% and 10% of these emissions. This pattern is due to the relatively small surface area occupied by waterbodies smaller than 1 km^2 (8% of the total surface area; Supplementary Table 13) compared with the larger share for waterbodies larger than 100 km^2 (70% of the total surface area; Supplementary Table 13), and despite the slightly higher area-weighted emission rates in small waterbodies (Supplementary Table 14).

Comparing the CO_2-equivalent contributions of each GHG with the total emission flux (Fig. 4), the CO_2 flux was the largest component for reservoirs ($p < 0.01$), contributing 53% of the total CO_2-equivalent emissions, with the remaining contributed by total CH_4 (41%) and N_2O (6%). For lakes, in contrast, the total CH_4 emissions were the highest ($p < 0.01$) and contributed 75% of the CO_2-equivalent lake emissions, with CO_2 (24%) and N_2O (1%) contributing the remaining. The wet-dry tropics had the highest fluxes across all GHGs and system types, alongside the (semi)arid regions for lakes and followed by the humid subtropics for reservoirs ($p < 0.01$; Fig. 4). This partly reflects the wet-dry tropics' largest surface areas for both lakes and reservoirs (Supplementary Table 13).

Our median total CH_4 flux estimate of 5.4 TgCH$_4$ yr^{-1} was 3.5 times smaller than the 18.8 TgCH$_4$ yr^{-1} from (sub)tropical lakes reported by Johnson et al.[15], who used a smaller total surface area than us (371×10^3 km^2 versus 616×10^3 km^2). This discrepancy is not due to substantial differences in diffusive fluxes between the two studies (Supplementary Table 7), but rather to the upscaling method: Johnson et al.[15] extrapolated mean fluxes, whereas we used medians in our bootstrapping, which we consider more robust to outliers[30] (Supplementary Discussion 3 and Supplementary Table 7). That previous study also included floodplain lakes (excluded here) and applied lower ebullition rates only in systems larger than 5,000 km^2, while we used a more conservative threshold of 1,000 km^2, based on the assumption that ebullition from deeper areas is likely to be negligible (undetectable at depths >5 m (refs. 50,51)). Using medians for our ebullition estimates may not fully capture rare, high-magnitude events. This choice was intentional to provide a conservative estimate, given the current data limitations, and we acknowledge that the actual flux could be higher. Indeed, using mean CH_4 ebullitive fluxes instead of medians, as in the case of Johnson et al.[15], would increase the total CH_4 flux estimate to 974.9 TgCH$_4$ yr^{-1}, an 180-fold difference compared with our estimate, highlighting how strongly the choice of central tendency (mean versus median) influences upscaling results[30]. Beyond collecting more ebullition data, there is a clear need for more transparent and comparable approaches to upscaling. Our downward revision is further supported by a recent assessment using a mechanistic model[52], which reported global CH_4 emissions from lakes that are roughly 50% lower than previous estimates[15,30]. Overall, our work represents a step towards reducing the large uncertainties that remain regarding global lake and reservoir CH_4 emissions[53] (Supplementary Discussion 3).

Our scaled CO_2 and N_2O estimates for standing waterbodies cannot be directly compared with previous work[28] as fluxes have not been specifically reported for the (sub)tropics. However, it is likely that our lake CO_2 emission estimates are lower than those from earlier studies, consistent with a recent analysis suggesting that CO_2 concentrations in African lakes and resulting emissions have previously been overestimated by an order of magnitude[18]. Our N_2O estimate of 0.03 TgN$_2$O yr^{-1} amounts to only 15% of previous global estimates[8,17] (both 0.20 TgN$_2$O yr^{-1}), supporting the view that the bulk of lake N_2O emissions is unlikely to originate from the (sub)tropics[8,18].

https://doi.org/10.1038/s44221-025-00522-8

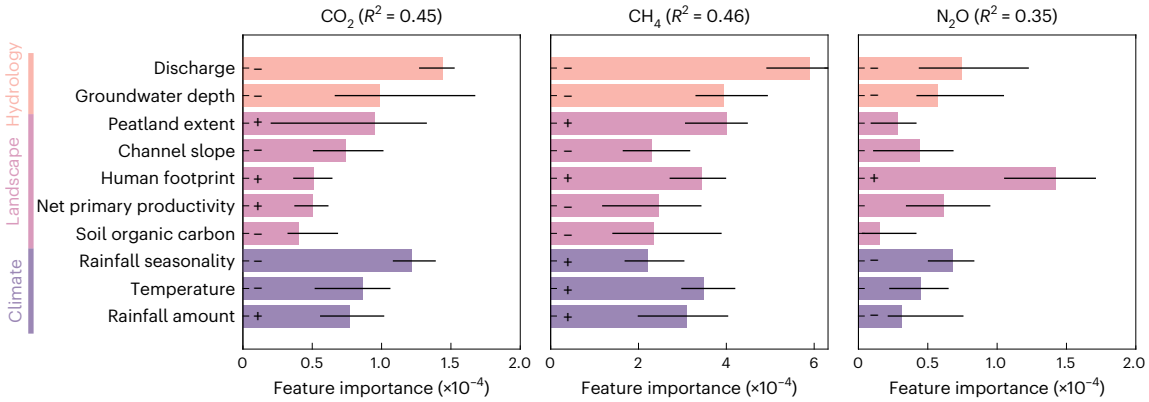

Fig. 3 | Importance of ten catchment attributes in predicting GHG concentrations in streams and rivers. Catchment attributes can explain the variability in measured CO_2, CH_4 and N_2O concentrations. Attributes include hydrological, landscape and climate variables. All ten catchment attributes were used as predictors in random forest models (see Methods). The R^2 values above each plot indicate the proportion of variance in GHG concentrations explained by the models. Bars represent median feature importance across 20 optimization runs of the models. Error bars indicate the interquartile range from these runs. The + and − signs on each bar indicate the direction of influence for each predictor; the absence of a sign indicates unclear or weak influences. Partial dependence plots provide further information on how each predictor influences GHG concentrations and are available in Supplementary Figs. 9–11. Analyses are based on n = 2,471 (CO_2), n = 2,027 (CH_4) and n = 644 (N_2O) independent site-level observations compiled from the database.

Table 2 | Total median GHG emissions for lakes and reservoirs for each climate zone of the (sub)tropics

Climate zone	CO_2 flux ($TgCO_2\,yr^{-1}$)	CH_4 diffusive flux ($TgCH_4\,yr^{-1}$)	CH_4 ebullitive flux ($TgCH_4\,yr^{-1}$)	N_2O flux ($TgN_2O\,yr^{-1}$)
Lakes				
Humid tropics	8.8 (3.8–18.7)	0.20 (0.10–0.33)	0.63 (0.20–1.09)	0.001 (0.000–0.003)
Wet-dry tropics	11.6 (5.2–26.4)	0.23 (0.13–0.35)	0.76 (0.25–1.22)	0.001 (0.000–0.004)
(Semi)arid (sub)tropics	11.1 (5.1–18.5)	0.22 (0.10–0.41)	0.84 (0.35–1.38)	0.001 (−0.000–0.004)
Humid subtropics	8.4 (3.9–13.6)	0.11 (0.07–0.21)	0.51 (0.17–0.88)	0.000 (−0.000–0.002)
Highland (sub)tropics	3.1 (1.6–5.4)	0.06 (0.03–0.10)	0.22 (0.09–0.35)	0.000 (−0.000–0.001)
Total lakes	42.9 (19.6–82.6)	0.82 (0.42–1.41)	2.96 (1.06–4.93)	0.003 (−0.000–0.013)
Reservoirs				
Humid tropics	9.0 (6.8–16.7)	0.04 (0.02–0.05)	0.15 (0.05–0.26)	0.003 (0.003–0.005)
Wet-dry tropics	24.3 (18.6–51.8)	0.10 (0.07–0.18)	0.45 (0.14–0.77)	0.010 (0.007–0.013)
(Semi)arid (sub)tropics	15.2 (11.4–26.1)	0.06 (0.04–0.11)	0.25 (0.09–0.41)	0.006 (0.005–0.008)
Humid subtropics	20.6 (15.2–38.0)	0.09 (0.06–0.15)	0.45 (0.15–0.74)	0.008 (0.006–0.011)
Highland (sub)tropics	2.4 (1.7–3.4)	0.01 (0.01–0.02)	0.05 (0.02–0.10)	0.001 (0.001–0.001)
Total reservoirs	71.4 (53.6–136.0)	0.30 (0.20–0.50)	1.35 (0.44–2.27)	0.028 (0.021–0.039)
Grand total	**114.4 (73.2–218.6)**	**1.12 (0.62–1.91)**	**4.31 (1.51–7.20)**	**0.032 (0.021–0.052)**

Values are based on a bootstrapping approach (see Methods) and the lower and upper bounds in parentheses correspond to Q1 and Q3, respectively. Surface areas were obtained using the SWOT Prior Lake Database[25] for systems larger than 0.01 km^2. The CH_4 ebullitive fluxes were estimated on the basis of the median flux from 286 observations scaled to the total surface area regardless of system size (see Methods). Further details on the distribution of surface areas per size class and climate zone are available in Supplementary Table 13.

Diverging size effects on lake and reservoir GHG emissions

Previous work has shown that CO_2 and CH_4 emissions from lakes and reservoirs tend to decrease with larger surface areas[2,28–30]. Our data revealed similar trends for both lakes and reservoirs, although not always significant (Fig. 5b,d,f and Supplementary Table 14). The decreasing pattern did not hold in large reservoirs (>10 km^2), which had significantly higher CO_2 and CH_4 fluxes than similarly sized lakes. Decreasing fluxes with increasing area may arise from small systems receiving high organic matter inputs and being more influenced by sediments and littoral zones[54], which together raise CO_2 and CH_4 levels[55]. In contrast, larger systems experience higher gas transfer velocities (Supplementary Table 15) due to greater fetch[56] and more stable seasonal stratification[57], which, together, reduce surface CO_2 and CH_4 levels (Supplementary Table 15). This reduction in larger systems is likely due to a combination of reduced inputs from the hypolimnion and increased sinks in the mixed layer (such as degassing for both gases, primary production for CO_2 and microbial oxidation for CH_4).

N_2O fluxes in lakes also varied consistently with lake size, but in the opposite direction, with the majority of systems smaller than 10 km^2 acting as sinks of atmospheric N_2O while larger systems were weak sources (Fig. 5f and Supplementary Table 14). In waterbodies with low dissolved inorganic nitrogen levels, such as the relatively pristine lakes of the humid tropics, N_2O levels are generally low due to removal through soil denitrification, resulting in limited inputs from groundwater, and further removal via sedimentary denitrification[18]. Unlike for lakes, we found consistently positive N_2O emissions across reservoir sizes, with no clear size effect (Fig. 5f). Increased N inputs from agricultural sources and flooded soils may explain these higher reservoir N_2O concentrations and emissions (Supplementary Tables 14 and 15). Nearly all (97%) our reservoir N_2O data came from southeast

https://doi.org/10.1038/s44221-025-00522-8

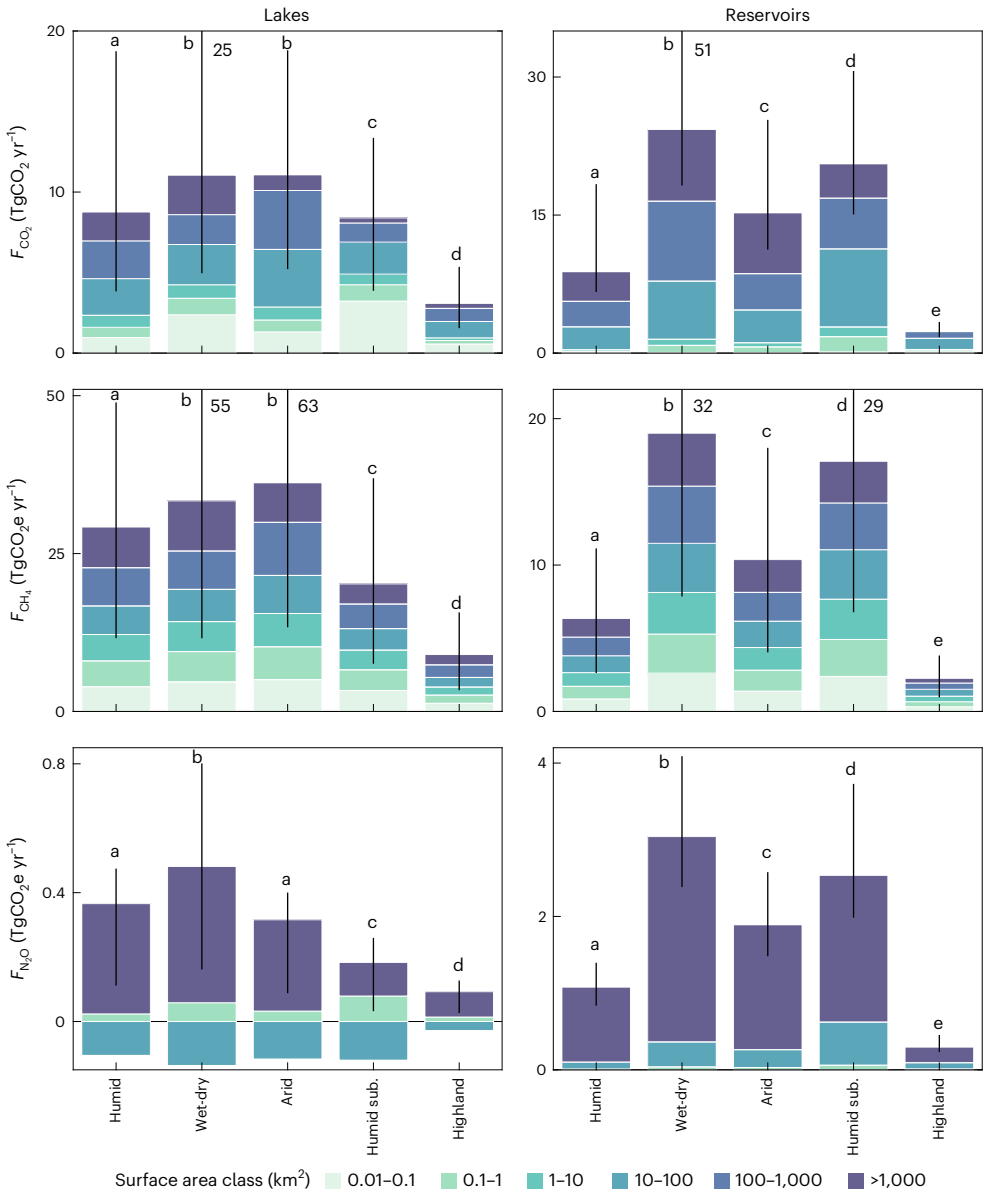

Fig. 4 | Contributions of CO_2, CH_4 and N_2O to the total modelled lake and reservoir emission flux. Median fluxes were estimated for lakes and reservoirs and for each climate zone. Lakes and reservoirs are binned by surface area class. Fluxes are expressed as CO_2-equivalents using 100-year global warming potential factors of 34 for CH_4 and 298 for N_2O (ref. 113). CH_4 fluxes include both diffusive and ebullitive fluxes. For N_2O, we merged size classes into three broader classes (<0.1, 0.1–10 and >10 km^2) to increase sample size (see Methods). Error bars indicate Q1 and Q3 based on propagated uncertainties. For clarity, some error bars have been truncated and the corresponding Q3 values are shown. Letters indicate significant differences between climate zones based on two-sided Kruskal–Wallis tests followed by pairwise, two-sided Wilcoxon rank-sum post hoc comparisons with Benjamini–Hochberg correction ($p < 0.01$) applied to bootstrapped flux distributions. Each plot has different y-axis scales.

China and India, where high levels of human alteration and eutrophication may explain the high fluxes[58–60].

We did not observe a strong or consistent effect of climate on median GHG fluxes, although CO_2 and CH_4 emissions tended to be higher in the humid tropics, and N_2O emissions were higher in the humid tropics and subtropics, as well as in the arid (sub)tropics (Fig. 5a,c and Supplementary Tables 16a,b). High CO_2 fluxes in the humid tropics may be linked to high terrestrial productivity in this region[61] and increased lake heterotrophy[18], whereas eutrophic waterbodies can be weak sources, or even sinks, of CO_2 (refs. 62,63). The drivers of GHG concentrations in lakes are multifaceted (for example, depth, surface area, productivity, connectivity with rivers and human disturbance) and while our dataset provides new insights, this complexity, combined with limited observations, remains an impediment to upscaling efforts[10,28,29].

Addressing observation gaps and future directions

Reducing uncertainties in key parameters such as surface area estimates, gas exchange rates and CH_4 ebullition will be essential to improve our estimates of (sub)tropical inland water emissions (Supplementary Discussion 4). Achieving this will also require the observation gaps that we identified across the (sub)tropics to be addressed. Despite new research adding valuable data, the coverage for both flowing and standing waters remains skewed towards the humid (sub)tropics, leaving gaps in more seasonal and (semi)arid environments (Fig. 1, Extended Data Fig. 3 and Supplementary Figs. 4–7). The scarcity of waterbodies in these drier areas cannot fully explain this pattern as we controlled for seasonal intermittency in river surface areas (see Methods). Low measurement density in drier regions may be related to

https://doi.org/10.1038/s44221-025-00522-8

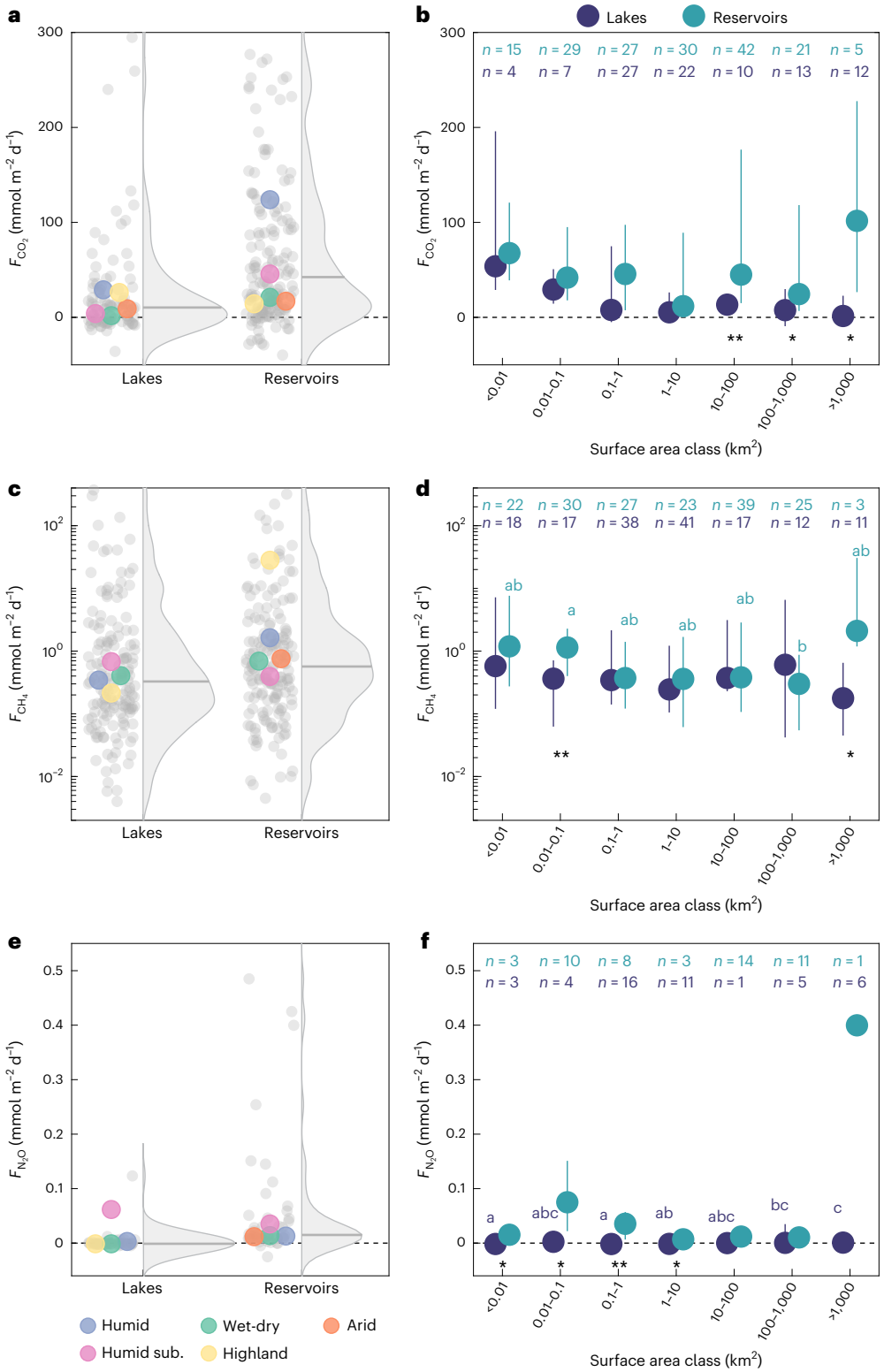

Fig. 5 | Distribution of CO_2, diffusive CH_4 and N_2O fluxes per unit area from lakes and reservoirs in the (sub)tropics. **a**,**c**,**e**, Fluxes of CO_2 (**a**), diffusive CH_4 (**c**) and N_2O (**e**) grouped by waterbody type. **b**,**d**,**f**, Median and interquartile range of fluxes of CO_2 (**b**), diffusive CH_4 (**d**) and N_2O (**f**) for lakes and reservoirs grouped by surface area bins (in km^2). In **a**, **c** and **e**, the grey horizontal bars on each density plot represent the medians across all climates and coloured circles represent the medians per climate zone. In **b**, **d** and **f**, the coloured circles represent the medians and the error bars the interquartile range. Some error bars may be hidden when smaller than the median circle. Black asterisks below groups indicate significant differences between lakes and reservoirs within the same size class, based on pairwise two-sided Kolmogorov–Smirnov tests (*$p < 0.05$ and **$p < 0.01$). Coloured letters above markers of the same waterbody type indicate significant differences across size classes based on two-sided Kruskal–Wallis tests followed by pairwise, two-sided Wilcoxon rank-sum post hoc comparisons with Benjamini–Hochberg correction ($p < 0.05$). The *n* values denote the number of systems, and the horizontal dashed lines in **a**, **b**, **e** and **f** indicate zero flux.

the historically limited focus on seasonal and intermittent waterbodies, despite emissions during dry periods being potentially important[64,65]. While our analysis suggests that emission rates are lower in drier, less productive regions than in the humid tropics, additional observations are needed to reduce uncertainty in global upscaling efforts.

Low-order streams are less represented than high-order rivers (Extended Data Fig. 3). For example, first- and second-order streams have 2.4 sites per 10^3 km^2 of wetted river surface area, whereas seventh- to tenth-order rivers have 11.6 sites per 10^3 km^2 of wetted river surface area. This discrepancy is noteworthy given the significance of GHG emissions from low-order streams[14,35,36,66,67]. Their under-representation in our dataset, combined with the high uncertainty in gas transfer velocity estimates for small streams (Supplementary Discussion 4), likely resulted in greater uncertainties in our emission estimates for these systems. In addition, there are few observations in larger lakes and reservoirs across all climate zones (Extended Data Fig. 3). The shortage of measurements in large systems, their disproportionate share of the global standing water surface area[25,68] and their substantial contribution to GHG emissions (Fig. 4) warrants the need for further observation efforts in waterbodies larger than 100 km^2.

The numerous drainage canals in peatlands of southeast Asia, which were not explicitly included in our analysis, are likely hotspots of GHG emissions[69] and represent an area of uncertainty. Using the estimated surface area of these canals[70] (157×10^3 km^2) and the median areal GHG fluxes from our meta-analysis (humid tropics; Supplementary Table 9), we estimated hypothetical emissions of approximately 785 TgCO$_2$ yr^{-1}, 2.4 TgCH$_4$ yr^{-1} and 0.06 TgN$_2$O yr^{-1}, a 23% increase on our CO$_2$-equivalent riverine estimates. While some of this flux is likely to have been captured in our analysis as canals overlap with the natural drainage network, these estimates are probably conservative as peatland cover tends to boost riverine emissions (Fig. 3). Given the expected expansion of drainage canals, more measurements in these systems and a better representation of their surface area in global river network products are needed.

The impact of human activities on GHGs in (sub)tropical inland waters also needs further scrutiny. The tropics are undergoing widespread land use changes due to agricultural and urban development[71,72], often alongside dam construction[73,74]. These changes are altering flow regimes[75] and the productivity of both terrestrial[72] and aquatic[76] ecosystems, with consequences for inland water GHG emissions[6,62,77]. The urban rivers of lower-income countries, for example, represent a large, potentially under-reported GHG source[46]. Our analysis illustrates the effect of human disturbance on N$_2$O emissions[78], yet predicting the response of inland waters to land use changes is hindered by limited GHG data, particularly for N$_2$O. Our database has fewer N$_2$O measurements than CO$_2$ and CH$_4$ across all climate zones and waterbodies (Extended Data Fig. 3), which contributed to greater uncertainties in our N$_2$O emission estimates. Our finding of substantial N$_2$O emission rates in (sub)tropical reservoirs calls for more detailed investigation.

Tropical rivers operate under very dynamic, flood-pulse-driven flow regimes, where a limited number of high flow events can account for the bulk of annual GHG emissions[79–81], particularly in seasonally dry areas. In lakes, mixing events triggered by storms can increase GHG emissions owing to weaker vertical density gradients compared with higher latitude systems[82]. Capturing these short-term, as well as seasonal and interannual, variations characteristic of (sub)tropical hydroclimates will require long-term data at high temporal resolution[83]. High-frequency in situ measurements of GHGs will also be key to capture differences in daytime and night-time emissions[84–87]. This temporal focus will contribute to a more holistic approach to the study of C and N cycles in the tropics, complementing efforts to integrate spatial connectivity across riparian wetlands, rivers and reservoirs[88–90]. In addition to the collection of new, preferably coordinated datasets, improving data accessibility will be pivotal to refine future estimates[91].

Conclusions

The (sub)tropics are incredibly diverse in terms of climate, landforms, vegetation and levels of human alteration. We have shown that this diversity translates into distinct differences in GHG concentrations and fluxes from inland waters across the region. Despite the lower total surface area occupied by flowing waters compared with standing waters (471×10^3 km^2 versus 616×10^3 km^2), flowing waters released 30 times more CO$_2$ (3,387 TgCO$_2$ yr^{-1} versus 114 TgCO$_2$ yr^{-1}), twice as much CH$_4$ (10.6 TgCH$_4$ yr^{-1} versus 5.4 TgCH$_4$ yr^{-1}) and 20 times more N$_2$O (0.62 TgN$_2$O yr^{-1} versus 0.03 TgN$_2$O yr^{-1}) than standing waters. Total emissions amounted to 4,238 TgCO$_2$e yr^{-1}, 93% of which were emitted by streams and rivers. The differences between flowing and standing waters were driven by large variations in areal flux rates between systems (Supplementary Tables 10 and 14).

The humid tropics and, to a lesser extent, the wet-dry tropics contributed the most to CO$_2$-equivalent emissions across the (sub) tropics. Our data also indicate that small headwater streams and large lakes and reservoirs were strong GHG emitters throughout the (sub) tropics, with first- to third-order streams contributing 75% of riverine CO$_2$-equivalent emissions and lakes and reservoirs larger than 100 km^2 contributing 55% of standing water CO$_2$-equivalent emissions.

While (sub)tropical regions account for 58% (flowing waters) and 20% (standing waters) of global wetted surface area, their contributions to global inland water GHG emissions based on the most recent global estimates[7,8,14,15,28] were only 46% and 8%, respectively (Extended Data Table 1). We attribute this downward revision of (sub) tropical fluxes to our use of a more extensive dataset, improved geospatial products and different upscaling approaches. Our lower CH$_4$ emission estimates compared with recent studies[7,15,30] may contribute to closing the gap between top-down and bottom-up estimates of global CH$_4$ emissions[53]. Nonetheless, our results suggest that (sub) tropical inland waters still released nearly three times the GHG emissions of inland waters of the northern cryosphere[92] at 1,500 TgCO$_2$e yr^{-1} (for a 100-year warming potential).

(Sub)tropical inland waters play a crucial role in global C and N budgets. Rising temperatures and increasing human disturbances in the (sub)tropics, both of which drive inland water GHG emissions, are expected to increase the contribution of these waters to global emissions. In this context, further efforts to monitor GHG emissions from (sub)tropical inland waters will be key to better understand and predict their role in global C and N budgets.

Methods

Literature data extraction

In our literature review, we used a hybrid approach, combining our a priori knowledge with an objective literature search. We first created a curated library of publications that included GHG data (CO$_2$, CH$_4$ and/or N$_2$O) from (sub)tropical inland waters. The curated library was aggregated over several weeks and discussed among the group of authors. It included Chinese-language university theses and publications available to the Chinese speakers within the group. This curated library was supplemented with a traditional literature review conducted in Web of Science, for which we used the following boolean query '(CH4 OR methane OR CO2 OR 'carbon dioxide' OR 'greenhouse gas*' OR N2O OR nitrous) AND (aquatic OR stream* OR creek* OR lake* OR reservoir* OR floodplain OR river* OR wetland* OR freshwater OR 'inland water*' OR pond* OR swamp*) AND (tropic* OR subtropic* OR (monsoon* NOT temperate))'. We excluded papers that did not fit the scope of this work and the last search was conducted during the revision of this paper in April 2025.

Our meta-analysis was based on a total of 517 peer-reviewed articles and 14 theses reporting GHG observations from across the (sub) tropical region. Our database contained 22,502 concentration and 11,129 flux measurements for flowing waterbodies, and 4,324 concentration and 5,404 flux measurements for standing waterbodies

(Supplementary Figs. 1–3). We assembled a total of 23,080, 14,550 and 5,297 measurements (flux and concentration) for CO_2, diffusive CH_4 and N_2O, respectively, as well as 432 ebullitive CH_4 flux measurements (146 and 286 for standing and flowing waters, respectively). The majority (66%) of these data were collected in the past 10 years (Extended Data Fig. 1). Our database was substantially larger than recent data compilations, for example, Johnson et al.[15] included CH_4 measurements from 80 standing waterbodies within latitudes between 34° S and 34° N, while we have data from 402 standing waterbodies (that is, 5 times more). Liu et al.[14] used CO_2 concentration data from 1,075 river sites between 34° S and 34° N, while we included 2,471 river sites (that is, 2.5 times more).

We carefully checked all of the published data and excluded observations with unclear methodology, apparent unit inconsistencies that we could not confidently resolve or data showing obvious outliers without justification. We then extracted data on GHG concentrations, fluxes and gas transfer velocities, as well as information on the methods used to obtain concentration (for example, sensor, gas chromatograph, indirect CO_2 estimates from pH and alkalinity) and flux (for example, floating chamber, eddy covariance and indirect via an empirical model of gas transfer velocity) measurements. Details on the proportion of direct versus indirect flux estimates and an assessment of method-related differences are provided in Supplementary Discussion 1. For references reporting CH_4 data, we noted whether the CH_4 flux was measured as diffusion, ebullition or both.

We also extracted ancillary data, including geographic coordinates, elevation, ecosystem type, stream order, discharge, lake surface area and any other reported physicochemical parameter (for example, temperature, pH, conductivity and dissolved organic/inorganic carbon). For each stream or river site, we reviewed the reported coordinates using Google Earth (https://earth.google.com/) and, if necessary, corrected them. We also manually extracted an estimate of channel width based on Google Earth. For observations collected from on-the-run river surveys, we accounted for potential spatial autocorrelation due to closely spaced measurements by applying a clustering algorithm to group nearby sampling points. We used the `dbscan` function in MATLAB (https://www.mathworks.com/products/matlab.html) to merge all sampling locations within 5 km of one another for river orders higher than 7. As our focus was on freshwater ecosystems, we excluded coastal and estuarine ecosystems based on salinity and tidal influence. We also excluded data from volcanic lakes with active magmatic activity as these lakes are characterized by CO_2 emissions several orders of magnitude higher than other lakes[93] but represent a very small fraction of crater lakes. To assess the spatiotemporal coverage of the data, we recorded the frequency of measurements and categorized each site according to its temporal resolution of sampling (from high-frequency observations to daily, weekly, monthly, seasonal, annual or single measurements). We further discuss the temporal resolution and seasonal coverage in Supplementary Discussion 2.

For each site, we extracted the climate class based on the latest iteration of the Köppen–Geiger classification[27]. We grouped the classes into five broad climate zones: humid tropics (tropical rainforest, Af and tropical monsoon, Am), wet-dry tropics (tropical savanna, Aw), (semi)arid (sub)tropics (desert hot, BWh; desert cold, BWk; steppe hot, BSh; steppe cold, BSk), humid subtropics (subtropical monsoon, Cwa and subtropical humid, Cfa) and highland (sub)tropics (subtropical highland monsoon, Cwb; humid oceanic, Cfb; humid continental warm, Dwb; humid continental cool, Dwc; frost, EF; tundra, ET; Extended Data Fig. 2). Because concentrations and flux measurements were reported in a wide range of units, we converted and homogenized all units to μmol l^{-1} (concentrations) and mmol m^{-2} d^{-1} (fluxes). To do this, we used known conversion factors and temperature-dependent Henry's constants for the three GHGs[94–96]. We also conducted several quality control steps, where each contributor reviewed and revised the data extractions of others. To assess differences in fluxes, concentrations and gas transfer velocities across stream orders, lake size classes, system types and climate zones, we conducted non-parametric analyses on medians using MATLAB. Due to deviations from normality, we used the Kruskal–Wallis test (`kruskalwallis`) for overall group comparisons, followed by pairwise Wilcoxon rank-sum post hoc tests (`ranksum`) with Benjamini–Hochberg correction. When comparing lakes and reservoirs within the same size class, we applied two-sample Kolmogorov–Smirnov tests (`kstest2`).

Riverine GHG flux upscaling

For each stream and river site in the database, we extracted catchment properties from a range of existing geospatial products. We used Hydrography90m[24], which includes headwater streams with a minimal upstream contributing area of 0.05 km^2, to obtain catchment area, stream order, channel slope and elevation. We used BasinATLAS[97] for attributes such as average air temperature, average rainfall, soil organic carbon content and human footprint[43] (a metric that includes direct and indirect human pressures such as population density, agricultural land and built environment). We used other products to compile annual net primary productivity[98] and peatland extent[99] as per Rocher-Ros et al.[7]. Peatland extent was chosen over the wetland extent variable available in BasinATLAS due to its higher spatial resolution. Lastly, we computed a rainfall seasonality index as per Feng et al.[100] using monthly rainfall values from BasinATLAS.

We used our refined coordinates and channel width estimates to accurately snap the sites onto the Hydrography90m river network and performed quality control by comparing reported catchment areas with those derived from Hydrography90m. We estimated the total river surface area covered by each stream order and for each climate zone based on the Global Reach-Level A priori Discharge Estimates for SWOT (GRADES) dataset[22] (Supplementary Table 8). Because of the resolution of GRADES, this approach did not capture first-order streams, which we estimated by extrapolating width and length using scaling relationships, as described by Liu et al.[14]. Lastly, to account for flow intermittency and the drying periods of river networks[101], we adjusted the total wetted river surface area by applying a weighting factor specific to each climate zone, following the procedure developed by Liu et al.[14] (Supplementary Table 8). GRADES was also used to estimate the mean annual run-off for each site in the database.

To avoid any location bias in our upscaling approach, where one site is over-represented due to repeated measurements, we first computed mean concentration and flux values for each site. We chose to use means rather than medians to preserve temporal variability at individual sites as medians could underestimate values by artificially flattening seasonal fluctuations. To expand the dataset of GHG fluxes, we then estimated fluxes at sites where only concentration data were available. To do this, we estimated the flow velocity using the relationship with discharge[14]. We calculated Schmidt numbers for each GHG[56] and used model 5 from Raymond et al.[102], which provided better fits than the piecewise approach used in previous work[14]. To evaluate how well this model reproduced measured fluxes, we compared modelled fluxes (based on the aforementioned model 5) to directly measure the fluxes obtained using floating chambers or gas tracers. When combining data across all three gases, a power-law regression yielded a coefficient of determination (R^2) of 0.73 (Supplementary Fig. 2).

The next step involved using a bootstrap approach to calculate medians and uncertainties for flux estimates across different subgroups of stream orders and climate zones. In this step, medians were preferred over means due to the small sample sizes in several subgroups, where mean-based bootstrapping would be highly sensitive to outliers and could produce unrealistically high estimates. We used the `bootstrp` function in MATLAB, drawing 1,000 bootstrap samples with replacement. For stream order and climate zone combinations with fewer than ten flux values, we applied the median flux value calculated for that stream order across all climate zones.

Uncertainties in total flux estimates account for uncertainties in both flux and surface area. Flux uncertainties were derived using MATLAB's `bootci` function with the 'bias-corrected and accelerated' method to extract Q1 and Q3. The resulting bootstrapped flux values were multiplied by the surface area corresponding to each stream order and climate zone combination. We considered uncertainties of ±30% in surface area estimates, higher than those commonly reported in global river maps[103], because we aimed to account for the greater uncertainty associated with the surface area of low-order streams (Supplementary Discussion 4). For each climate zone and stream order combination, we scaled the upper bound of the flux estimate using the upper range of the area estimate and the lower bound of the flux estimate using the lower range of the area estimate. To propagate uncertainties, we summed the upper and lower bounds of each climate zone and stream order. We have reported uncertainties as ranges based on these propagated upper and lower bounds.

Few studies have quantified ebullitive CH_4 fluxes (n_obs = 146 ebullitive flux estimates versus n_obs = 3,711 diffusive flux estimates in our riverine database). This imbalance has also been observed in global CH_4 databases and analyses[30,38]. In our case, the ebullitive and diffusive components of CH_4 fluxes were positively related on a log–log scale across flowing and standing waterbodies ($R^2 = 0.36$, $p < 0.0001$; Supplementary Fig. 12). While previous studies[7] have used this relationship to upscale ebullitive fluxes from diffusive fluxes, the limited number of ebullitive measurements in our case was insufficient to derive a reliable estimate. Instead, we applied the more robust, river-specific relationship reported by Rocher-Ros et al.[7] to estimate riverine ebullitive CH_4 fluxes. We used the goodness of fit from that study ($R^2 = 0.34$) to estimate uncertainties.

Random forest modelling

We applied random forest models to explain the variability in GHG concentrations in our database. While we initially intended to assess the drivers of GHG fluxes, the number of direct flux measurements (particularly for N_2O) was too limited for a meaningful analysis. Because higher concentrations are associated with higher fluxes (Extended Data Fig. 4), we can reasonably assume that the drivers identified for concentrations are also relevant for fluxes. Ten predictor variables were selected and grouped into three categories, namely, climate (mean rainfall, mean temperature and seasonality index), landscape (channel slope, human footprint, peatland extent, net primary productivity and soil organic carbon) and hydrological (mean discharge and groundwater depth) variables. Stream order and catchment area were excluded due to their strong correlations with run-off, with Spearman's rank correlation coefficients of 0.91 and 0.98, respectively. No other predictors had correlation coefficients higher than 0.7 or lower than −0.7 (Supplementary Fig. 8), suggesting that the individual contributions of each predictor can be distinguished.

Before modelling, both predictor and response variables were log-transformed if non-normally distributed, and predictors were normalized to zero mean and unit variance. A random forest model (MATLAB function `fitrensemble`) was then trained using a built-in Bayesian hyperparameter optimization with 25 evaluations and a 5-fold cross-validation. This optimization step was repeated over 20 runs to ensure robust feature importance. Four key parameters were adjusted, including the number of learning cycles (range of 300–1,600), the minimum leaf size (range of 2–25), the maximum number of splits (range of 10–100) and the number of predictors sampled at each split (range of 1–10). Feature importance (MATLAB function `predictorImportance`) and the partial dependence of each variable (MATLAB function `partialDependence`) were used to assess the influence of individual predictors on GHG concentrations. The uncertainties in the models' outputs were determined by extracting the interquartile range for each feature importance value based on 20 optimization runs.

Standing waterbody flux upscaling

Standing waterbodies were classified as either natural (lakes and natural ponds, referred to as 'lakes') or artificial (reservoirs and man-made ponds, referred to as 'reservoirs') based on the description given in each paper. Because of the difficulty in assessing their surface area and the high spatiotemporal variability in GHG emissions[104], we excluded (sub) tropical wetlands from our analysis (Supplementary Discussion 5). We used the HydroLAKES database[105] to estimate the surface area of each standing waterbody in the database. For waterbodies not included in HydroLAKES (168 out of 395), we extracted their surface areas directly from the reference or, in some cases, manually digitized them using Google Earth. Similar to the approach used for streams and rivers, we computed mean concentration and flux values for individual waterbodies to avoid any location bias in the data and preserve temporal dynamics across systems[30].

We estimated the total surface area covered by standing waterbodies for each climate zone using the SWOT Prior Lake Database[25], which maps waterbodies down to 0.01 km^2. We used the Global Dam Watch database[23] to classify the waterbodies as either lakes or reservoirs (Supplementary Table 13). One exception was Lake Victoria, which we assigned to the 'lake' class. For sites where only GHG concentrations were reported, we estimated fluxes using gas transfer velocity parameterizations and the annual average wind speed data from the WorldClim 2 database[106]. While annual averages may not capture short-term fluctuations or extreme wind events, the seasonal variability of wind speed is relatively low in the tropics compared with mid-latitudes. We took the mean of fluxes based on the two empirical models[107,108] that provided the best fits between modelled and measured fluxes (Supplementary Fig. 3). We then upscaled diffusive GHG fluxes separately for lakes and reservoirs using six logarithmic surface area bins (0.01–0.1, 0.1–1, 1–10, 10–100, 100–1,000 and >1,000 km^2), a common approach in global scaling studies[30]. Because of the low number or absence of observations when separating flux data by size class and climate zone (Fig. 5), we binned the data independently of climate. The variability of our upscaled GHG fluxes accounts for differences in surface areas between climate zones, rather than capturing the variability in flux data across these zones. While this approach may underestimate fluxes from warmer climate zones such as the humid and wet-dry tropics, it reduces the influence of potential outliers due to low sample size (Supplementary Discussion 3).

For reservoirs larger than 1,000 km^2, given the high uncertainty associated with the small number of systems (n_systems = 5) and the potential for overestimation caused by their higher median values (see text and Fig. 5), we combined the flux values from this class with those from the next lower size class (100–1,000 km^2). This approach makes our estimates more conservative and might not fully capture the potentially high fluxes from large, newly commissioned reservoirs. At the other end of the size range, there are limited GHG flux observations for small size classes, but these systems, albeit numerous, represent a low contribution to the total surface area of reservoirs. Due to the smaller number of systems with N_2O data, we used broader surface area bins (< 0.1, 0.1–10, >10 km^2) for this gas, allowing for larger sample sizes per bin (7 < n_system < 17) and thus improving the robustness of our upscaled estimates.

Similar to our approach for rivers, we computed median fluxes and Q1 and Q3 across the different size bins using the `bootstrp` and `bootci` functions in MATLAB, with 1,000 bootstrap samples drawn with replacement. We then multiplied the bootstrapped values by the cumulative surface area of each bin and climate zone combination. We considered uncertainties of ±10% in lake/reservoir surface area estimates, reflecting the difference between estimates from the Prior Lake Database[25] and other global products[105,109]. Uncertainties were propagated the same way as for rivers.

To estimate ebullitive CH_4 fluxes, we did not group the data by size class due to limited data availability. Instead, we applied the

overall median flux from our dataset of 286 measurements ($2.01^{14.64}_{0.04}$ mmol m^{-2} d^{-1}) uniformly across the entire surface area of lakes and reservoirs, regardless of size. Following a similar approach to Johnson et al.[15], we adjusted fluxes for large systems (>1,000 km^2) by applying 10% of the median flux value, assuming that ebullition is negligible in the deep areas of larger systems[50,51]. We estimated uncertainties in the total ebullitive flux using a bootstrapping procedure (1,000 samples drawn with replacement) considering ±100% variability around the median flux and ±10% uncertainty in surface area estimates.

We did not use random forest models to assess the drivers of GHG concentrations in lakes and reservoirs because a large portion (44%) of waterbodies, including nearly all those smaller than 0.1 km^2, were not included in HydroLAKES, making it difficult to extract catchment attributes. While factors such as reservoir age can explain some of the variability in GHG measurements, with fluxes often strongly decreasing over time after commissioning[110–112], we were not able to assess this effect due to the lack of available data.

Reporting summary

Further information on research design is available in the Nature Portfolio Reporting Summary linked to this article.

Data availability

The dataset generated as part of this paper is available via Github at https://github.com/ClementDuvert/GHG.flux.tropics/tree/main/Data.

Code availability

The code used in the analyses is available via Github at https://github.com/ClementDuvert/GHG.flux.tropics.

References

1. Cole, J. J. et al. Plumbing the global carbon cycle: integrating inland waters into the terrestrial carbon budget. *Ecosystems* **10**, 172–185 (2007).
2. Raymond, P. A. et al. Global carbon dioxide emissions from inland waters. *Nature* **503**, 355–359 (2013).
3. Tranvik, L. J., Cole, J. J. & Prairie, Y. T. The study of carbon in inland waters—from isolated ecosystems to players in the global carbon cycle. *Limnol. Oceanogr. Lett.* **3**, 41–48 (2018).
4. Yao, Y. et al. Increased global nitrous oxide emissions from streams and rivers in the Anthropocene. *Nat. Clim. Change* **10**, 138–142 (2020).
5. Regnier, P., Resplandy, L., Najjar, R. G. & Ciais, P. The land-to-ocean loops of the global carbon cycle. *Nature* **603**, 401–410 (2022).
6. Battin, T. J. et al. River ecosystem metabolism and carbon biogeochemistry in a changing world. *Nature* **613**, 449–459 (2023).
7. Rocher-Ros, G. et al. Global methane emissions from rivers and streams. *Nature* **621**, 530–535 (2023).
8. Li, Y. et al. Increased nitrous oxide emissions from global lakes and reservoirs since the pre-industrial era. *Nat. Commun.* **15**, 942 (2024).
9. Tian, H. et al. Increased terrestrial carbon export and CO_2 evasion from global inland waters since the preindustrial era. *Glob. Biogeochem. Cycles* **37**, e2023GB007776 (2023).
10. Lauerwald, R. et al. Inland water greenhouse gas budgets for RECCAP2: 1. state-of-the-art of global scale assessments. *Glob. Biogeochem. Cycles* **37**, e2022GB007657 (2023).
11. Abril, G. et al. Amazon River carbon dioxide outgassing fuelled by wetlands. *Nature* **505**, 395–398 (2014).
12. Borges, A. V. et al. Globally significant greenhouse-gas emissions from African inland waters. *Nat. Geosci.* **8**, 637–642 (2015).
13. Borges, A. V. et al. Variations in dissolved greenhouse gases (CO_2, CH_4, N_2O) in the Congo River network overwhelmingly driven by fluvial-wetland connectivity. *Biogeosciences* **16**, 3801–3834 (2019).
14. Liu, S. et al. The importance of hydrology in routing terrestrial carbon to the atmosphere via global streams and rivers. *Proc. Natl Acad. Sci. USA* **119**, e2106322119 (2022).
15. Johnson, M. S., Matthews, E., Du, J., Genovese, V. & Bastviken, D. Methane emission from global lakes: new spatiotemporal data and observation-driven modeling of methane dynamics indicates lower emissions. *J. Geophys. Res. Biogeosci.* **127**, e2022JG006793 (2022).
16. Marzadri, A. et al. Global riverine nitrous oxide emissions: the role of small streams and large rivers. *Sci. Total Environ.* **776**, 145148 (2021).
17. Lauerwald, R. et al. Natural lakes are a minor global source of N_2O to the atmosphere. *Glob. Biogeochem. Cycles* **33**, 1564–1581 (2019).
18. Borges, A. V. et al. Greenhouse gas emissions from African lakes are no longer a blind spot. *Sci. Adv.* **8**, eabi8716 (2022).
19. Bastviken, D., Tranvik, L. J., Downing, J. A., Crill, P. M. & Enrich-Prast, A. Freshwater methane emissions offset the continental carbon sink.*Science* **331**, 50 (2011).
20. Lauerwald, R., Laruelle, G. G., Hartmann, J., Ciais, P. & Regnier, P. A. G. Spatial patterns in CO_2 evasion from the global river network. *Glob. Biogeochem.Cycles* **29**, 534–554 (2015).
21. Marzolf, N. S. & Ardón, M. Ecosystem metabolism in tropical streams and rivers: a review and synthesis. *Limnol. Oceanogr.* **66**, 1627–1638 (2021).
22. Lin, P. et al. Global reconstruction of naturalized river flows at 2.94 million reaches. *Water Resour. Res.* **55**, 6499–6516 (2019).
23. Mulligan, M. et al. Global Dam Watch: curated data and tools for management and decision making. *Environ. Res. Infrastruct. Sustain.* **1**, 033003 (2021).
24. Amatulli, G. et al. Hydrography90m: a new high-resolution global hydrographic dataset. *Earth Syst. Sci. Data* **14**, 4525–4550 (2022).
25. Wang, J. et al. The Surface Water and Ocean Topography Mission (SWOT) Prior Lake Database (PLD): lake mask and operational auxiliaries. *Water Resour. Res.* **61**, e2023WR036896 (2025).
26. Osland, M. J. et al. Tropicalization of temperate ecosystems in North America: the northward range expansion of tropical organisms in response to warming winter temperatures. *Glob. Change Biol.* **27**, 3009–3034 (2021).
27. Beck, H. E. et al. High-resolution (1 km) Köppen-Geiger maps for 1901–2099 based on constrained CMIP6 projections. *Sci. Data* **10**, 724 (2023).
28. DelSontro, T., Beaulieu, J. J. & Downing, J. A. Greenhouse gas emissions from lakes and impoundments: upscaling in the face of global change. *Limnol. Oceanogr. Lett.* **3**, 64–75 (2018).
29. Deemer, B. R. & Holgerson, M. A. Drivers of methane flux differ between lakes and reservoirs, complicating global upscaling efforts. *J. Geophys. Res. Biogeosci.* **126**, e2019JG005600 (2021).
30. Rosentreter, J. A. et al. Half of global methane emissions come from highly variable aquatic ecosystem sources. *Nat. Geosci.* **14**, 225–230 (2021).
31. Chiriboga, G. & Borges, A. V. Andean headwater and piedmont streams are hot spots of carbon dioxide and methane emissions in the Amazon basin. *Commun. Earth Environ.* **4**, 76 (2023).
32. Schneider, C. L. et al. Carbon dioxide (CO_2) fluxes from terrestrial and aquatic environments in a high-altitude tropical catchment. *J. Geophys. Res. Biogeosci.* **125**, e2020JG005844 (2020).
33. Lehner, B. et al. Mapping the world's inland surface waters: an upgrade to the Global Lakes and Wetlands Database (GLWD v2). *Earth Syst. Sci. Data* **17**, 2277–2329 (2025).
34. Wallin, M. B. et al. Evasion of CO_2 from streams—the dominant component of the carbon export through the aquatic conduit in a boreal landscape. *Glob. Change Biol.* **19**, 785–797 (2013).
35. Hotchkiss, E. R. et al. Sources of and processes controlling CO_2 emissions change with the size of streams and rivers. *Nat. Geosci.* **8**, 696–699 (2015).

36. Marx, A. et al. A review of CO_2 and associated carbon dynamics in headwater streams: a global perspective. *Rev. Geophys.* **55**, 560–585 (2017).
37. Mwanake, R. M. et al. Basin-scale estimates of greenhouse gas emissions from the Mara River, Kenya: importance of discharge, stream size, and land use/land cover. *Limnol. Oceanogr.* **67**, 1776–1793 (2022).
38. Stanley, E. H. et al. GRiMeDB: the Global River Methane Database of concentrations and fluxes. *Earth Syst. Sci. Data* **15**, 2879–2926 (2023).
39. Tamooh, F. et al. Dynamics of dissolved inorganic carbon and aquatic metabolism in the Tana River basin, Kenya. *Biogeosciences* **10**, 6911–6928 (2013).
40. Müller, D. et al. Lateral carbon fluxes and CO_2 outgassing from a tropical peat-draining river. *Biogeosciences* **12**, 5967–5979 (2015).
41. Duvert, C., Butman, D. E., Marx, A., Ribolzi, O. & Hutley, L. B. CO_2 evasion along streams driven by groundwater inputs and geomorphic controls. *Nat. Geosci.* **11**, 813–818 (2018).
42. Moustapha, M. et al. Partitioning carbon sources between wetland and well-drained ecosystems to a tropical first-order stream—implications for carbon cycling at the watershed scale (Nyong, Cameroon). *Biogeosciences* **19**, 137–163 (2022).
43. Venter, O. et al. Global terrestrial Human Footprint maps for 1993 and 2009. *Sci. Data* **3**, 160067 (2016).
44. Zhang, W., Li, H., Xiao, Q. & Li, X. Urban rivers are hotspots of riverine greenhouse gas (N_2O, CH_4, CO_2) emissions in the mixed-landscape Chaohu Lake basin. *Water Res.* **189**, 116624 (2021).
45. Liu, S. et al. Human activities reshape greenhouse gas emissions from inland waters. *Glob. Change Biol.* **31**, e70139 (2025).
46. Xu, W. et al. Globally elevated greenhouse gas emissions from polluted urban rivers. *Nat. Sustain.* **7**, 938–948 (2024).
47. Teodoru, C. R. et al. Dynamics of greenhouse gases (CO_2, CH_4, N_2O) along the Zambezi River and major tributaries, and their importance in the riverine carbon budget. *Biogeosciences* **12**, 2431–2453 (2015).
48. Zeikus, J. G. & Winfrey, M. R. Temperature limitation of methanogenesis in aquatic sediments. *Appl. Environ. Microbiol.* **31**, 99–107 (1976).
49. Yvon-Durocher, G. et al. Methane fluxes show consistent temperature dependence across microbial to ecosystem scales. *Nature* **507**, 488–491 (2014).
50. DelSontro, T., Boutet, L., St-Pierre, A., del Giorgio, P. A. & Prairie, Y. T. Methane ebullition and diffusion from northern ponds and lakes regulated by the interaction between temperature and system productivity. *Limnol. Oceanogr.* **61**, S62–S77 (2016).
51. Wik, M., Crill, P. M., Varner, R. K. & Bastviken, D. Multiyear measurements of ebullitive methane flux from three subarctic lakes. *J. Geophys. Res. Biogeosci.* **118**, 1307–1321 (2013).
52. Zhuang, Q. et al. Current and future global lake methane emissions: a process-based modeling analysis. *J. Geophys. Res. Biogeosci.* **128**, e2022JG007137 (2023).
53. Saunois, M. et al. Global methane budget 2000–2020.*Earth Syst. Sci. Data Discuss.* **2024**, 1–147 (2024).
54. Khatun, S. et al. Long-range transport of littoral methane explains the metalimnetic methane peak in a large lake. *Limnol. Oceanogr.* **69**, 2095–2108 (2024).
55. Staehr, P. A., Baastrup-Spohr, L., Sand-Jensen, K. & Stedmon, C. Lake metabolism scales with lake morphometry and catchment conditions. *Aquat. Sci.* **74**, 155–169 (2012).
56. Wanninkhof, R. Relationship between wind speed and gas exchange over the ocean revisited. *Limnol. Oceanogr. Methods* **12**, 351–362 (2014).
57. Kling, G. W. Comparative transparency, depth of mixing, and stability of stratification in lakes of Cameroon, West Africa. *Limnol. Oceanogr.* **33**, 27–40 (1988).
58. Le, C. et al. Eutrophication of lake waters in China: cost, causes, and control. *Environ. Manage.* **45**, 662–668 (2010).
59. Huang, J. et al. How successful are the restoration efforts of China's lakes and reservoirs?. *Environ. Int.* **123**, 96–103 (2019).
60. Kundu, S., Coumar, M. V., Rajendiran, S., Rao, A. & Rao, A. S. Phosphates from detergents and eutrophication of surface water ecosystem in India. *Curr. Sci.* **108**, 1320–1325 (2015).
61. Beer, C. et al. Terrestrial gross carbon dioxide uptake: global distribution and covariation with climate. *Science* **329**, 834–838 (2010).
62. Ran, L. et al. Substantial decrease in CO_2 emissions from Chinese inland waters due to global change. *Nat. Commun.* **12**, 1730 (2021).
63. Wen, Z. et al. Re-estimating China's lake CO_2 flux considering spatiotemporal variability. *Environ. Sci. Ecotechnol.* **19**, 100337 (2024).
64. Keller, P. S. et al. Global CO_2 emissions from dry inland waters share common drivers across ecosystems. *Nat. Commun.* **11**, 2126 (2020).
65. Paranaíba, J. R. et al. Cross-continental importance of CH_4 emissions from dry inland-waters. *Sci. Total Environ.* **814**, 151925 (2022).
66. Horgby, Å et al. Unexpected large evasion fluxes of carbon dioxide from turbulent streams draining the world's mountains. *Nat. Commun.* **10**, 4888 (2019).
67. Wallin, M. B. et al. Carbon dioxide and methane emissions of Swedish low-order streams—a national estimate and lessons learnt from more than a decade of observations. *Limnol. Oceanogr. Lett.* **3**, 156–167 (2018).
68. Verpoorter, C., Kutser, T., Seekell, D. A. & Tranvik, L. J. A global inventory of lakes based on high-resolution satellite imagery. *Geophys. Res. Lett.* **41**, 6396–6402 (2014).
69. Bowen, J. C., Wahyudio, P. J., Anshari, G. Z., Aluwihare, L. I. & Hoyt, A. M. Canal networks regulate aquatic losses of carbon from degraded tropical peatlands. *Nat. Geosci.* **17**, 213–218 (2024).
70. Dadap, N. C. et al. Drainage canals in southeast Asian peatlands increase carbon emissions. *AGU Adv.* **2**, e2020AV000321 (2021).
71. Lambin, E. F., Geist, H. J. & Lepers, E. Dynamics of land-use and land-cover change in tropical regions. *Annu. Rev. Environ. Resour.* **28**, 205–241 (2003).
72. Gibbs, H. K. et al. Tropical forests were the primary sources of new agricultural land in the 1980s and 1990s. *Proc. Natl Acad. Sci. USA* **107**, 16732–16737 (2010).
73. Zarfl, C., Lumsdon, A. E., Berlekamp, J., Tydecks, L. & Tockner, K. A global boom in hydropower dam construction. *Aquat. Sci.* **77**, 161–170 (2015).
74. Winemiller, K. O. et al. Balancing hydropower and biodiversity in the Amazon, Congo, and Mekong. *Science* **351**, 128–129 (2016).
75. Kayitesi, N. M., Guzha, A. C. & Mariethoz, G. Impacts of land use land cover change and climate change on river hydro-morphology—a review of research studies in tropical regions. *J. Hydrol.* **615**, 128702 (2022).
76. Tanaka, Y., Minggat, E. & Roseli, W. The impact of tropical land-use change on downstream riverine and estuarine water properties and biogeochemical cycles: a review. *Ecol. Process.* **10**, 40 (2021).
77. Calamita, E. et al. Unaccounted CO_2 leaks downstream of a large tropical hydroelectric reservoir. *Proc. Natl Acad. Sci.* **118**, e2026004118 (2021).
78. Chan, C. N. et al. Experimental ecosystem eutrophication causes offsetting effects on emissions of CO_2, CH_4, and N_2O from agricultural reservoirs. *Environ. Sci. Technol.* **58**, 7045–7055 (2024).
79. Almeida, R. M., Pacheco, F. S., Barros, N., Rosi, E. & Roland, F. Extreme floods increase CO_2 outgassing from a large Amazonian river. *Limnol. Oceanogr.* **62**, 989–999 (2017).

80. Duvert, C. et al. Net landscape carbon balance of a tropical savanna: relative importance of fire and aquatic export in offsetting terrestrial production. *Glob. Change Biol.* **26**, 5899–5913 (2020).
81. Geeraert, N., Omengo, F. O., Borges, A. V., Govers, G. & Bouillon, S. Shifts in the carbon dynamics in a tropical lowland river system (Tana River, Kenya) during flooded and non-flooded conditions. *Biogeochemistry* **132**, 141–163 (2017).
82. Borges, A. V. et al. Spatial and temporal variations of dissolved CO_2, CH_4 and N_2O in Lakes Edward and George (East Africa). *J. Great Lakes Res.* **49**, 229–245 (2023).
83. Dean, J. F. & Battin, T. J. Future directions for river carbon biogeochemistry observations. *Nat. Water* **2**, 219–222 (2024).
84. Sieczko, A. K. et al. Diel variability of methane emissions from lakes. *Proc. Natl Acad. Sci.* **117**, 21488–21494 (2020).
85. Gómez-Gener, L. et al. Global carbon dioxide efflux from rivers enhanced by high nocturnal emissions. *Nat. Geosci.* **14**, 289–294 (2021).
86. Rudberg, D. et al. Diel variability of CO_2 emissions from northern lakes. *J. Geophys. Res. Biogeosci.* **126**, e2021JG006246 (2021).
87. Woodrow, R. L. et al. Enhanced stream greenhouse gas emissions at night and during flood events. *Limnol. Oceanogr. Lett.* **9**, 276–285 (2024).
88. Abril, G. & Borges, A. V. Ideas and perspectives: carbon leaks from flooded land: do we need to replumb the inland water active pipe? *Biogeosciences* **16**, 769–784 (2019).
89. Prairie, Y. T. et al. Greenhouse gas emissions from freshwater reservoirs: what does the atmosphere see? *Ecosystems* **21**, 1058–1071 (2018).
90. Hotchkiss, E. R., Sadro, S. & Hanson, P. C. Toward a more integrative perspective on carbon metabolism across lentic and lotic inland waters. *Limnol. Oceanogr. Lett.* **3**, 57–63 (2018).
91. Smits, A. P. et al. Too much and not enough data: challenges and solutions for generating information in freshwater research and monitoring. *Ecosphere* **16**, e70205 (2025).
92. Song, C. et al. Inland water greenhouse gas emissions offset the terrestrial carbon sink in the northern cryosphere. *Sci. Adv.* **10**, eadp0024 (2024).
93. Pérez, N. M. et al. Global CO_2 emission from volcanic lakes. *Geology* **39**, 235–238 (2011).
94. Plummer, L. N. & Busenberg, E. The solubilities of calcite, aragonite and vaterite in CO_2-H_2O solutions between 0 and 90 °C, and an evaluation of the aqueous model for the system $CaCO_3$-CO_2-H_2O. *Geochim. Cosmochim. Acta* **46**, 1011–1040 (1982).
95. Wiesenburg, D. A. & Guinasso, N. L. Jr. Equilibrium solubilities of methane, carbon monoxide, and hydrogen in water and sea water. *J. Chem. Eng. Data* **24**, 356–360 (1979).
96. Weiss, R. F. & Price, B. A. Nitrous oxide solubility in water and seawater. *Mar. Chem.* **8**, 347–359 (1980).
97. Linke, S. et al. Global hydro-environmental sub-basin and river reach characteristics at high spatial resolution. *Sci. Data* **6**, 283 (2019).
98. Running, S. W. & Zhao, M. *Daily GPP and Annual NPP (MOD17A2/A3) Products NASA Earth Observing System MODIS Land Algorithm—MOD17 User's Guide* 1–28 (MODIS Land Team, 2015).
99. Melton, J. R. et al. A map of global peatland extent created using machine learning (Peat-ML). *Geosci. Model Dev.* **15**, 4709–4738 (2022).
100. Feng, X., Porporato, A. & Rodriguez-Iturbe, I. Changes in rainfall seasonality in the tropics. *Nat. Clim. Change* **3**, 811–815 (2013).
101. Messager, M. L. et al. Global prevalence of non-perennial rivers and streams. *Nature* **594**, 391–397 (2021).
102. Raymond, P. A. et al. Scaling the gas transfer velocity and hydraulic geometry in streams and small rivers. *Limnol. Oceanogr. Fluids Environ.* **2**, 41–53 (2012).
103. Allen, G. H. & Pavelsky, T. M. Global extent of rivers and streams. *Science* **361**, 585–588 (2018).
104. Melack, J. M. et al. Challenges regionalizing methane emissions using aquatic environments in the Amazon Basin as examples. *Front. Environ. Sci.* **10**, 866082 (2022).
105. Messager, M. L., Lehner, B., Grill, G., Nedeva, I. & Schmitt, O. Estimating the volume and age of water stored in global lakes using a geo-statistical approach. *Nat. Commun.* **7**, 13603 (2016).
106. Fick, S. E. & Hijmans, R. J. WorldClim 2: new 1-km spatial resolution climate surfaces for global land areas. *Int. J. Climatol.* **37**, 4302–4315 (2017).
107. Cole, J. J. & Caraco, N. F. Atmospheric exchange of carbon dioxide in a low-wind oligotrophic lake measured by the addition of SF6. *Limnol. Oceanogr.* **43**, 647–656 (1998).
108. Vachon, D. & Prairie, Y. T. The ecosystem size and shape dependence of gas transfer velocity versus wind speed relationships in lakes. *Can. J. Fish. Aquat. Sci.* **70**, 1757–1764 (2013).
109. Pi, X. et al. Mapping global lake dynamics reveals the emerging roles of small lakes. *Nat. Commun.* **13**, 5777 (2022).
110. Abril, G. et al. Carbon dioxide and methane emissions and the carbon budget of a 10-year old tropical reservoir (Petit Saut, French Guiana). *Glob. Biogeochem. Cycles* **19**, GB4007 (2005).
111. Barros, N. et al. Carbon emission from hydroelectric reservoirs linked to reservoir age and latitude. *Nat. Geosci.* **4**, 593–596 (2011).
112. Soued, C., Harrison, J. A., Mercier-Blais, S. & Prairie, Y. T. Reservoir CO_2 and CH_4 emissions and their climate impact over the period 1900–2060. *Nat. Geosci.* **15**, 700–705 (2022).
113. IPCC *Climate Change 2013: The Physical Science Basis* (eds Stocker, T. F. et al.) (Cambridge Univ. Press, 2013).

Acknowledgements

This research was supported by the Australian Research Council through grant DE220100852 awarded to C.D. Our effort to compile this database began during the 2021 Annual Meeting of the Society for Freshwater Science, session S11 'Greenhouse gases in tropical streams, rivers, lakes and wetlands: current work and future research needs'. We thank the meeting organizers for facilitating the session. E.C. acknowledges support from the European Space Agency as part of the Climate Change Initiative fellowship (ESA ESRIN/contract no. 4000133621/20/I/NB). M.N.M acknowledges support from the National Science Foundation (DEB-1950832).

Author contributions

C.D. and N.S.M. jointly oversaw the administration of the project. C.D., N.S.M., A.V.B., E.C., A.L., J.A.R. and G.R.-R. designed the study. All authors took part in data extraction from the literature and quality control of the extracted data. C.D. performed the analyses, with significant contributions from G.R.-R. for the riverine component and from A.V.B. and E.C. for the lake/reservoir component. C.D. wrote the initial draft of the paper with major input from A.V.B. All authors reviewed and edited the paper before submission.

Competing interests

The authors declare no competing interests.

Additional information

Extended data is available for this paper at https://doi.org/10.1038/s44221-025-00522-8.

Supplementary information The online version contains supplementary material available at https://doi.org/10.1038/s44221-025-00522-8.

Correspondence and requests for materials should be addressed to Clément Duvert, Alberto V. Borges or Nicholas S. Marzolf.

Peer review information *Nature Water* thanks Matthew Bogard and the other, anonymous, reviewer(s) for their contribution to the peer review of this work.

[1]Research Institute for the Environment and Livelihoods, Charles Darwin University, Darwin, Northern Territory, Australia. [2]College of Science and Engineering, James Cook University, Cairns, Queensland, Australia. [3]Chemical Oceanography Unit, University of Liège, Liege, Belgium. [4]Department of Surface Waters, Eawag, Swiss Federal Institute of Aquatic Science and Technology, Kastanienbaum, Switzerland. [5]Department of Geosciences, Eberhard Karls University of Tübingen, Tübingen, Germany. [6]Department of Forest Ecology and Management, Swedish University of Agricultural Sciences, Umeå, Sweden. [7]Department of Ecology and Environmental Sciences, Umeå University, Umeå, Sweden. [8]Department of Environmental Radioactivity and Monitoring, Federal Institute of Hydrology (BfG), Koblenz, Germany. [9]Faculty of Science and Engineering, Southern Cross University, Lismore, New South Wales, Australia. [10]Key Laboratory of Water and Sediment Sciences of MOE, State Key Laboratory of Water Environment Simulation, School of Environment, Beijing Normal University, Beijing, China. [11]Asian School of the Environment, Nanyang Technological University, Singapore, Singapore. [12]WasserCluster Lunz—Biological Station, Lunz am See, Austria. [13]Department of Functional and Evolutionary Ecology, University of Vienna, Vienna, Austria. [14]Department of Earth and Environmental Sciences, University of Waterloo, Waterloo, Ontario, Canada. [15]Géosciences Environnement Toulouse, Université Paul Sabatier, Toulouse, France. [16]Department of Natural Resources and the Environment, University of New Hampshire, Durham, NH, USA. [17]Department of Ecology and Genetics, Limnology, Uppsala University, Uppsala, Sweden. [18]Soil and Water Management Research Unit, United States Department of Agriculture, Agricultural Research Service, Saint Paul, MN, USA. [19]Institute for Environmental Sciences, RPTU Kaiserslautern-Landau, Landau, Germany. [20]Agrosphere (IBG3), Forschungszentrum Jülich, Jülich, Germany. [21]Institute for Meteorology and Climate Research, Atmospheric Environmental Research, Karlsruhe Institute of Technology, Garmisch-Partenkirchen, Germany. [22]Department of Ecology, Radboud Institute for Biological and Environmental Sciences, Radboud University, Nijmegen, The Netherlands. [23]Department of Geography, The University of Hong Kong, Hong Kong, China. [24]Groupe de Recherche Interuniversitaire en Limnologie, Département des Sciences Biologiques, Université du Québec à Montréal, Montréal, Quebec, Canada. [25]Institute of Surface-Earth System Science, School of Earth System Science, Tianjin University, Tianjin, China. [26]Department of Geography, University of North Carolina at Chapel Hill, Chapel Hill, NC, USA. [27]State Key Laboratory of Estuarine and Coastal Research, East China Normal University, Shanghai, China. [28]Department of Biological Sciences, Virginia Polytechnic Institute and State University, Blacksburg, VA, USA. [29]Woodwell Climate Research Center, Falmouth, MA, USA. [30]Amazon Environmental Research Institute, Brasília, Brazil. [31]Stroud Water Research Center, Avondale, PA, USA. [32]Jones Center at Ichauway, Newton, GA, USA. ✉e-mail: clem.duvert@cdu.edu.au; alberto.borges@uliege.be; nick.marzolf@jonesctr.org

https://doi.org/10.1038/s44221-025-00522-8

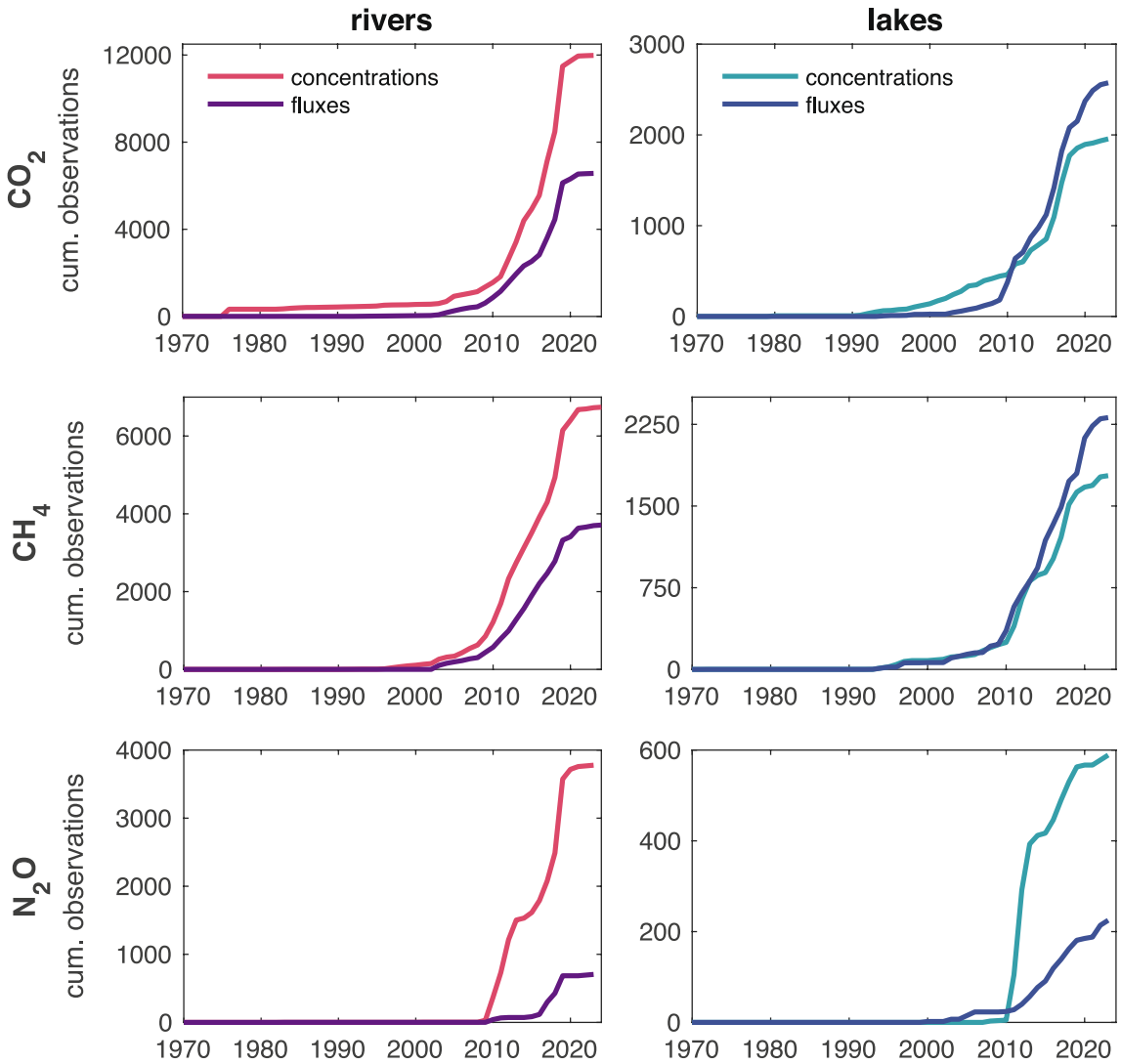

Extended Data Fig. 1 | Cumulative number of concentration and flux measurements through time. All measurements, including repeated measurements at single sites, are considered here. In total, 67% of the riverine data and 61% of the lake data were collected in the past ten years (that is since 2014). For rivers, these percentages per gas and measurement are 72, 59, and 60% for CO_2, CH_4 and N_2O concentrations, and 70, 65, and 90% for CO_2, CH_4 and N_2O fluxes, respectively. For lakes, percentages are 63, 54, and 33% for CO_2, CH_4 and N_2O concentrations, and 66, 65, and 75% for CO_2, CH_4 and N_2O fluxes, respectively.

https://doi.org/10.1038/s44221-025-00522-8

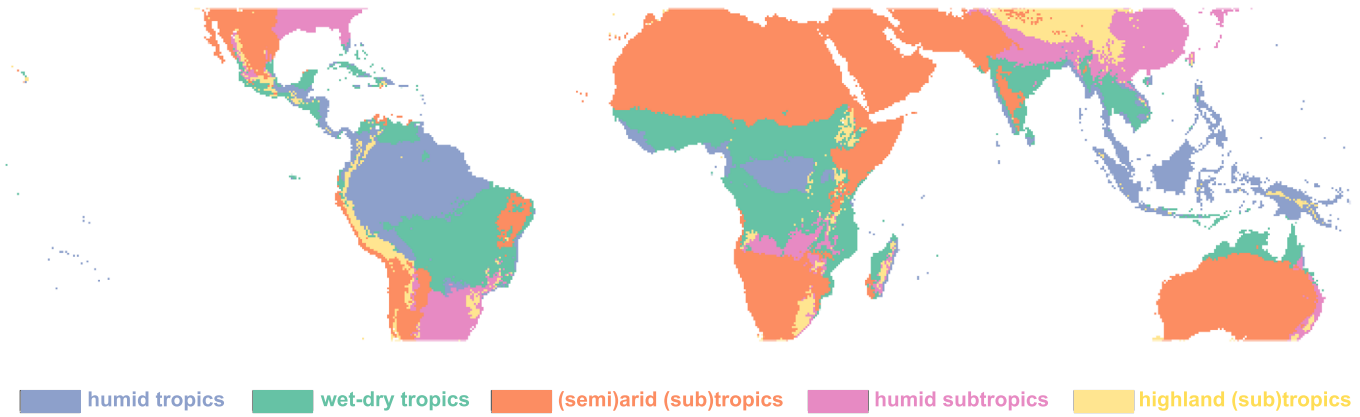

Extended Data Fig. 2 | Simplified Köppen-Geiger (sub)tropical climate zones. Simplified Köppen-Geiger climate zones as used in this study. The cut-off latitudes are 34°S and 34°N. Figure adapted from ref. 27 under a Creative Commons license CC BY 4.0.

https://doi.org/10.1038/s44221-025-00522-8

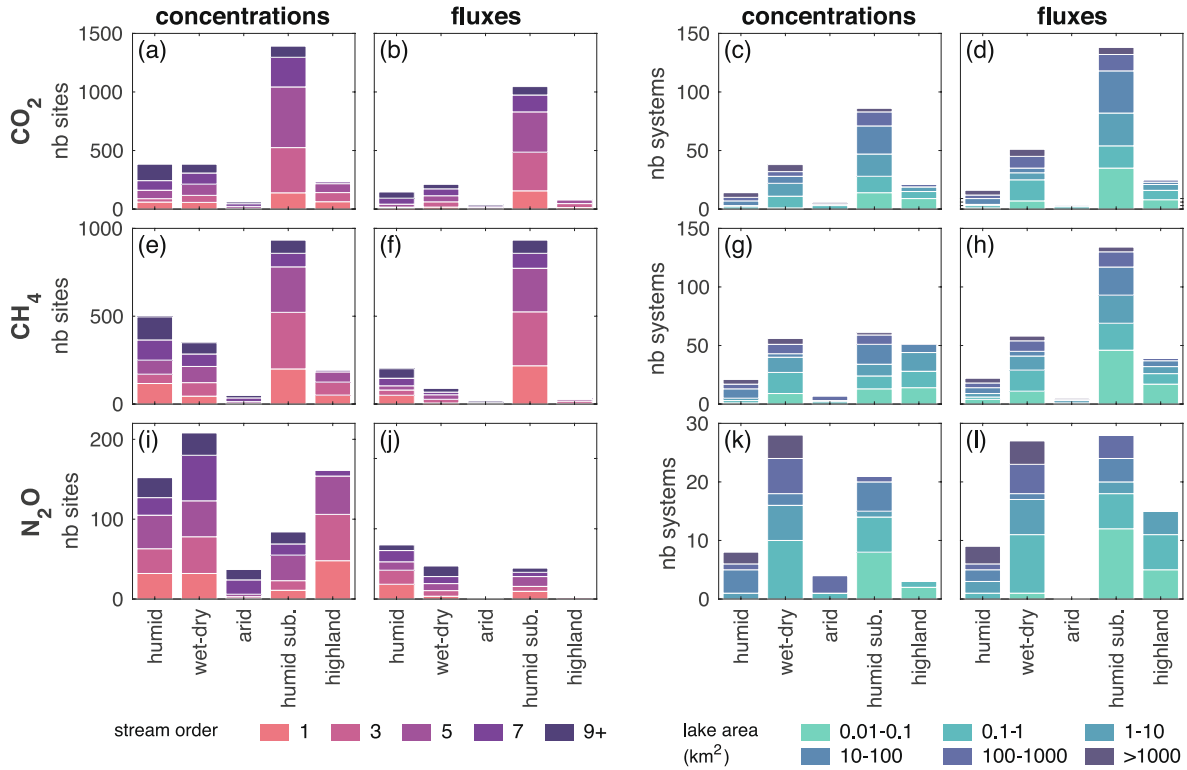

Extended Data Fig. 3 | Number of sites and systems with at least one measurement across gases, size classes and climate zones. Number of sites (flowing waters, left panel) and systems (standing waters, right panel) with at least one measurement of CO_2 concentration (**a**,**c**) and flux (**b**,**d**), CH_4 concentration (**e**,**g**) and flux (**f**,**h**), and N_2O concentration (**i**,**k**) and flux (**j**,**l**). Further details on spatial and temporal data coverage are available in Discussion S2.

https://doi.org/10.1038/s44221-025-00522-8

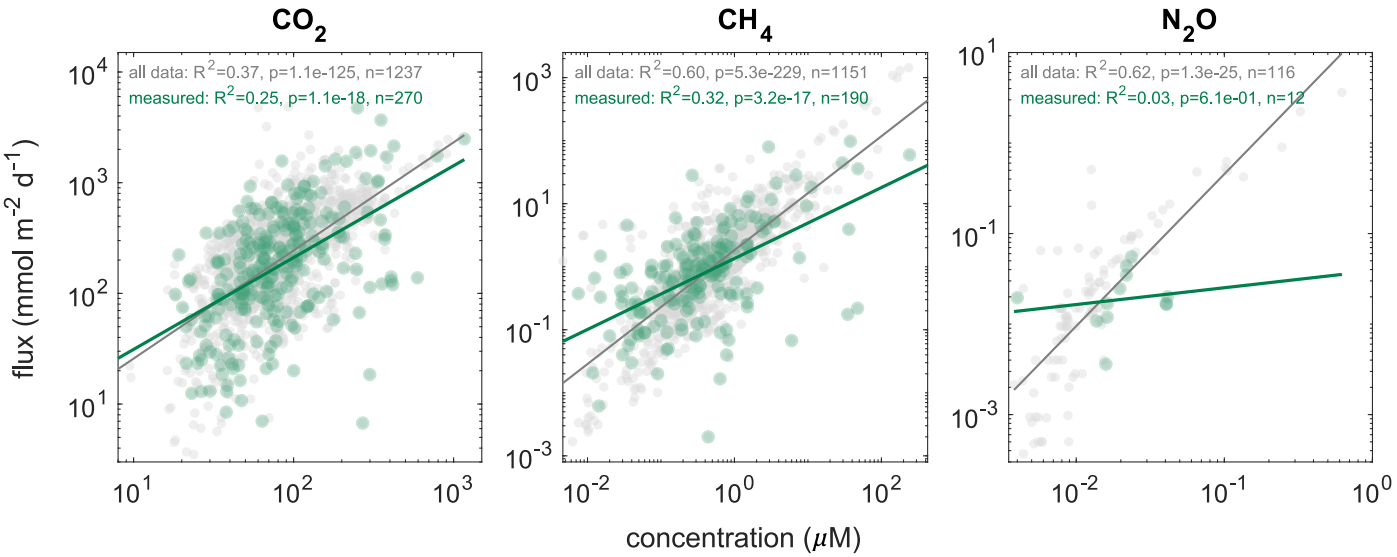

Extended Data Fig. 4 | Relationship between CO_2, diffusive CH_4, and N_2O fluxes and concentrations in flowing waters. Data points representing all flux estimates (both direct and indirect, see Discussion S1) are shown in light grey, while the green points correspond to direct flux estimates only. The grey and green lines represent power-law regressions fitted to the respective datasets. The positive relationships observed for CO_2 and CH_4 indicate that gas concentration is a strong control on emissions. Although no clear relationship is evident for direct N_2O measurements (likely due to the low sample size; n_sites=12), the indirect N_2O data suggest a similar behaviour to the other two GHGs. Reported p-values correspond to two-sided tests of the null hypothesis that the regression slope equals zero. No adjustments were made for multiple comparisons.

https://doi.org/10.1038/s44221-025-00522-8

Extended Data Table 1 | Comparison of median (sub)tropical inland water GHG emission estimates from this study with global inland water GHG emissions reported in the literature

	Waterbody type	Surface area (10^3 km^2)	CO_2 (Tg CO_2 yr^{-1})	CH_4 (Tg CH_4 yr^{-1})	N_2O (Tg N_2O yr^{-1})	Total (Tg CO_2-eq yr^{-1})
World	flowing	811	7,330[14]	27.9[7]	0.801[8]	**8,517**
	standing	3097	1,930[28]	52[15,114]	0.203[8]	**3,758**
(Sub)tropics (34°S to 34°N)	flowing	471 (58%)	3,387 (46%)	10.6 (38%)	0.615 (77%)	**3,931 (46%)**
	standing	616 (20%)	114 (6%)	5.4 (10%)	0.032 (16%)	**307 (8%)**

Comparison of median (sub)tropical inland water GHG emission estimates from this study with global inland water GHG emissions reported in the literature. The total CO_2-equivalent emissions were obtained considering a 100-yr global warming potential. Percentages in parentheses correspond to the assumed percent contribution of (sub)tropical inland waters to global emissions.